

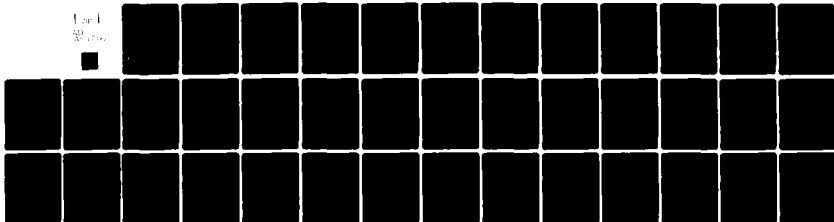
AD-A111 792

VIRGINIA POLYTECHNIC INST AND STATE UNIV BLACKSBURG --ETC F/6 20/4
THREE-DIMENSIONAL VISCOUS SHOCK-LAYER ANALYSIS OF LAMINAR OR TU--ETC(U)
MAY 81 B DENYSK

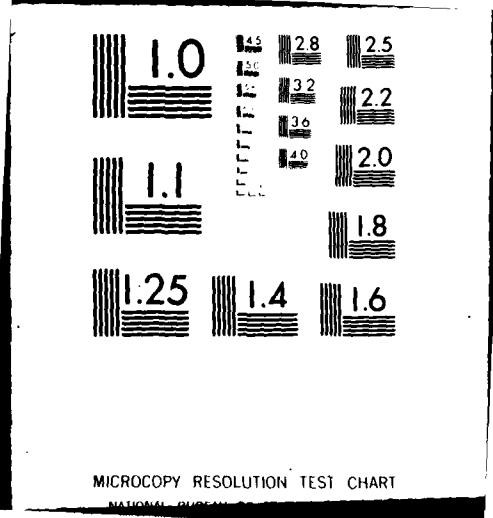
UNCLASSIFIED

NL

For
info



END
DATE
FILMED
4-82
DTIC



MICROCOPY RESOLUTION TEST CHART

NATIONAL BUREAU OF STANDARDS-1963-A

2

THREE-DIMENSIONAL VISCOUS SHOCK-LAYER ANALYSIS
OF LAMINAR OR TURBULENT FLOWS IN CHEMICAL EQUILIBRIUM

R. R. Thareja,* K. Y. Szema,** C. H. Lewis†

Virginia Polytechnic Institute and State University
Aerospace and Ocean Engineering Department
Blacksburg, Virginia

and

B. Denysyk†

EG&G
Dahlgren, Virginia

14 MAY 81

ABSTRACT

A method has been developed to predict three-dimensional hypersonic laminar or turbulent shock-layer flows for perfect gas or equilibrium air. A two-layer eddy-viscosity model is used for the turbulent regime. The thermodynamic and transport properties for air are obtained by interpolation within a two-dimensional table or from curve-fit data. Comparisons are made for air in chemical equilibrium and perfect gas for a seven-degree half-angle spherically blunted cone at various flight altitudes with a cold, moderately cool and an adiabatic wall for angles of attack up to twenty degrees. Wall heat transfer, wall pressure, force and moment coefficients and execution times are compared for some sample cases. This method can be used to predict viscous flow in chemical equilibrium over axisymmetric reentry vehicles at angles of attack up to 25 degrees.

INTRODUCTION

There is renewed interest in the problem of computing the hypersonic flow past a blunt body under flight conditions. Due to the current interest in the improved accuracy of ballistic and lifting reentry vehicles, a perfect gas model can no longer accurately predict the thermodynamic and transport properties required for inviscid and viscous flowfield analyses. Earlier investigators

*Graduate Student
**Research Associate
†Professor
‡Department Head

This document has been approved for public release and sale; its distribution is unlimited.

MAR 3 1982

AD A111792
FILE COPY

used a table look-up procedure¹ or curve-fit data² to model the thermodynamic and transport properties of air in chemical equilibrium for viscous boundary-layer flows.

Reentry vehicles operate through a wide range of flow conditions. The complex flowfield is bounded by the body and the bow shock. Crossflow separation may be present, and the viscous effects may predominate over the entire flowfield. The full Navier-Stokes equations are elliptic in all three space directions, and a numerical solution is difficult and requires large computing times and storage. For moderately high values of Reynolds number, there is no need to solve the full Navier-Stokes equations.³ The classical approach of dividing the flowfield into a viscous boundary-layer region and an outer inviscid region becomes inaccurate for reentry flowfields due to the presence of viscous effects throughout the entire flowfield. The parabolized Navier-Stokes (PNS) approach³ uses a parabolic approximation in the streamwise direction. This involves large matrix solutions, and the computing times are still quite large. The viscous shock-layer (VSL) approach⁴ developed by Murray and Lewis for three-dimensional flows is parabolic in both the streamwise and crossflow directions. Since the crossflow momentum equation is parabolic, the crossflow separated region on the leeward side cannot be treated. The solution for the windward region up to crossflow separation is accurate, and the computing times are relatively small. In the viscous shock-layer solution, the entire flowfield from the body to the shock is treated with a uniform set of equations. The problems associated with the displacement thickness interaction and edge conditions are eliminated, with vorticity interaction present in the inviscid + boundary-layer approach. As a result, the viscous shock-layer method treats all higher-order boundary-layer effects (displacement, vorticity interaction, longitudinal and transverse curvature, including proper matching conditions) in a straight-forward and consistent manner, making the viscous shock-layer approach especially attractive for design studies.

Recently, a numerical method was developed to predict laminar, transitional and/or turbulent hypersonic flows for a perfect gas⁵ over a blunt body at angle of attack. In that approach a two-layer eddy-viscosity model proposed by Cebeci⁶ and the transition model developed by Dhawan and Narasimha⁷ were used. This method has been extended to include the effect of air in chemical equilibrium. Results from a table look-up procedure and curve-fit methods have been compared with those from a perfect gas analysis. The table look-up procedure, described later, is known to model the thermodynamic properties of air quite accurately, while the transport properties are curve-fits of Hansen⁸ data.

Numerical solutions are presented for a seven-degree half-angle spherically blunted cone at a flight velocity of 20,000 ft/sec at altitudes of 40,000, 80,000 and 160,000 ft with a cold (540R), moderately cool (3600R) and an adiabatic wall for angles of attack up to twenty degrees. Wall heat-transfer, wall pressure, force and moment coefficients, center of pressure locations and execution times are compared for perfect gas and air in chemical equilibrium for some sample cases.

ANALYSIS

The basic, three-dimensional, viscous shock-layer equations are derived from the steady Navier-Stokes equations in a surface-oriented coordinate system

(s,n,φ). The governing equations for turbulent flow are developed using methods analogous to those presented in References 9 and 10. The normal velocity v and normal coordinate n are assumed to be of order ϵ , and second-order terms are retained in the s-momentum, φ-momentum and energy equations. The nondimensional turbulent-conservative form of the equations in a body-oriented coordinate system can be found in Reference 5.

EQUATION OF STATE

$$\rho = \rho(p,h)$$

For a perfect gas, the above equation has the analytical form:

$$\rho = \gamma p / [(\gamma-1)T]$$

For a gas in chemical equilibrium, the functional relation may be given by a table or an approximating analytical expression (curve-fit) as discussed in the section on thermodynamic and transport properties.

The same equations are valid for laminar flow if the turbulent eddy-viscosity ϵ^+ is set to zero.

For perfect gas flows, since the Prandtl number is not a function of n , it can be taken out of the derivative in the energy equation. For flows in chemical equilibrium, the Prandtl number is a function of pressure and enthalpy and thus of n ; therefore, it must be retained within the derivative term.

BOUNDARY CONDITIONS

Appropriate boundary conditions at the body surface and the shock must be specified for the set of governing equations. At the body surface or wall, no-slip and no temperature jump conditions are used. Thus, $u_w = v_w = w_w = 0$, and the wall temperature or heat-transfer rate is specified. The conditions immediately behind the shock are obtained from the Rankine-Hugoniot relations.

EDDY-VISCOSITY MODEL

For turbulent flow a two-layer eddy-viscosity model introduced by Cebeci⁶ consisting of an inner law based upon Prandtl's mixing-length concept and the Klebanoff¹¹-Clauser¹² expression for the outer law is used. Further details on the eddy-viscosity model can be found in Reference 5.

THERMODYNAMIC AND TRANSPORT PROPERTIES

For a perfect gas, the thermodynamic properties for specific heat and enthalpy can be expressed as

$$C_p = \gamma R / (\gamma-1)$$

$$h = C_p T$$

The viscosity is calculated from Sutherland's viscosity law:

$$\mu = 2.27 \text{ E-8 } T^{3/2} / (T + 198.6) \text{ slug/ft-sec}$$

The Prandtl number is assumed constant everywhere.

For air in chemical equilibrium a table look-up procedure or curve-fit data is used to provide the thermodynamic and transport properties as a function of the pressure and enthalpy.

TABLE LOOK-UP

A two-dimensional table was generated for the properties using the method developed by Miner, Anderson and Lewis.¹ For a given pressure and temperature, the enthalpy and density are determined using the reservoir calculations of Lordi.¹⁴ The viscosity is obtained by curve-fits from the Wilke semi-empirical formula,¹ while the Prandtl number is obtained by interpolation of the Hansen data.⁸

COHEN CURVE-FITS

Curve-fit data are based on Cohen's fit² of Hansen's tables⁸ for the transport properties and Moeckel tables¹⁵ for the thermodynamic properties of equilibrium air.

Density: The enthalpy dependence of the density is given by the curve-fit:

$$\frac{\rho_E}{\rho} = 1.0 - 1.0477 \left[1.0 - \left(\frac{h}{h_E} \right)^{0.6123} \right]$$

This fit is reasonably good for the enthalpy range $0.0152 \leq h/h_E \leq 2.0$. The maximum deviation in this range is about 25 percent at low enthalpy, and the average deviation for all data is about six percent.

The pressure dependence is given by the following:

$$\frac{\rho_E}{\rho_C} = 0.0294 \left(\frac{p}{p_C} \right)^{0.965}$$

This fit has a deviation of less than one-half percent over the range of pressures $10^{-4} \leq p/p_C \leq 10$.

Viscosity: The enthalpy dependence for the viscosity-density product is given by the curve-fit:

$$\frac{\rho_E \mu_E}{\rho \mu} = 1.0 - 1.0213 \left[1.0 - \left(\frac{h}{h_E} \right)^{0.3329} \right]$$

This fit has better agreement than that for the density. The maximum deviation over the enthalpy range $0.0152 \leq h/h_E \leq 2.0$ is about 8 percent and the average deviation is about three percent.

For the pressure dependence the following was used:

$$\frac{\rho_E \mu_E}{\rho_C \mu_C} = 0.225 \left(\frac{p}{p_C} \right)^{0.992}$$

This fit too has a deviation of about one-half percent.

Prandtl Number: The dependence of Prandtl number on pressure is neglected, and its variation with enthalpy is assumed to be of the form shown in Figure 2, which is a fit of Hansen's data.⁸ A pre-condition for the validity of an effective Prandtl number is that the gas must be in local thermodynamic equilibrium.

BADE CURVE-FITS

The density curve-fits from Cohen² are not in good agreement at low enthalpy. Better values of density are obtained using curve-fits suggested by Bade¹⁶

$$\frac{\rho}{\rho_B} = \left(\frac{p}{p_B} \right) \left(\frac{h}{h_B} \right)^{-x}$$

where,

$$x = 0.70 + 0.04 \log_{10} (p/p_B) \text{ if } 31.9 < h/RT_0 \leq 480$$

$$x = 0.94 \text{ if } h/RT_0 \leq 31.9$$

The fits have a maximum deviation of seven percent.

The viscosity and Prandtl number are then evaluated as in the Cohen curve-fits.

REFERENCE QUANTITIES IN CURVE-FITS

The following reference quantities were used in the calculations:

$$h_E = 2.119 \times 10^8 \text{ ft}^2/\text{sec}^2 = 8465 \text{ Btu/lbm}$$

$$p_C = 1.0 \text{ atm}$$

$$\mu_C = 3.584 \times 10^{-7} \text{ slugs/ft-sec}$$

$$\rho_C = 2.498 \times 10^{-3} \text{ slugs/ft}^3$$

$$\rho_B = 0.01 \text{ lb/ft}^3$$

$$h_B = 1080 \text{ Btu/lb} = 31.9 RT_0$$

$$p_B = 1.0 \text{ atm}$$



| | |
|--------------------|-------------------------------------|
| Checked For | <input checked="" type="checkbox"/> |
| Reviewed | <input type="checkbox"/> |
| Approved | <input type="checkbox"/> |
| Identification | <input type="checkbox"/> |
| BY | |
| Distribution/ | |
| Availability Codes | |
| Avail and/or | |
| Special | |

A

METHOD OF SOLUTION

Davis¹⁷ presented an implicit finite-difference method to solve the viscous shock-layer equations for axially symmetric flows. Murray and Lewis⁴ extended the method of solution to three-dimensional, high angle of attack conditions. The present method of solution is identical to that of Murray and Lewis. Therefore, only an overview of the solution procedure is presented here.

The equations are written in the standard form

$$A_0 \frac{\partial^2 W}{\partial \eta^2} + A_1 \frac{\partial W}{\partial \eta} + A_2 W + A_3 + A_4 \frac{\partial W}{\partial s} + A_5 \frac{\partial W}{\partial \phi} = 0$$

The derivatives are evaluated by the finite-difference expressions used by Frieders and Lewis¹⁸ and substituted into the parabolic equation giving the standard finite-difference form. The difference equation can be solved by the method developed by Richtmyer.

The continuity and normal momentum equations are solved by a similar method, but they are coupled together. Finally, the shock-standoff distance is evaluated by integrating the continuity equation as discussed by Murray and Lewis.⁴

The solution begins on the spherically-blunted nose by obtaining an axisymmetric solution in the wind-fixed coordinate system. At a specified location, the axisymmetric solution is rotated into the body-fixed coordinates and used as the initial profile for the three-dimensional solution. The three-dimensional solution begins on the windward plane and marches around the body obtaining a converged solution at each ϕ step. After completing a sweep in ϕ , the procedure then steps downstream in s and begins the next ϕ sweep. At each point the equations are solved in the following order: (i) ϕ -momentum, (ii) energy, (iii) s -momentum, (iv) integration of continuity for n_{sh} and (v) the coupled continuity and normal momentum equations.

RESULTS AND DISCUSSION

The freestream conditions used for the three altitudes are tabulated in Table 1, while the sample cases presented are shown in Table 2. The flow was assumed to be turbulent at 40,000 feet and laminar at 80,000 and 160,000 feet altitudes. The dimensions of the seven-degree half-angle spherically blunted cone are shown in Figure 1. The angles of attack considered were 0, 2, 10 and 20 degrees. The three wall conditions were a cold wall (540R), a cool wall (3600R) and an adiabatic wall.

TEST CASE RESULTS

A wide range of conditions was attempted, but since the variations were similar, only a few sample results are presented.

There is a significant change in the shock standoff distance for perfect gas and air in chemical equilibrium (Figure 3). The shock-layer thickness is

nearly the same for all options of the equilibrium properties.

Case A ($\alpha = 0$ degrees):

The streamwise variation of wall pressure with altitude shows very little differences (Figure 4) at 40,000 and 80,000 feet altitudes, but lower values are predicted for 160,000 feet. These values are nearly identical for all the gas models except within the nose region.

The streamwise variation of wall heat-transfer rate is shown in Figure 5 for all the cases. In general, the perfect gas and table look-up values are the lowest and highest respectively, with the Cohen and Bade values lying in between.

The variation of streamwise skin-friction coefficient shows trends similar to those for the wall heat-transfer rate. For some cases, the Cohen and Bade results do not lie within the band of perfect gas and table look-up values.

The force and moment data (Table 3) show a nine percent difference in the axial force coefficients from the perfect gas and table look-up results, while these differences are quite small for the Cohen and Bade results.

Case B ($\alpha = 2$ degrees)

The variation of the wall pressure for the windward plane is shown in Figure 7. The pressures from the table look-up and Bade options are nearly identical. On the spherical nose, the differences between perfect gas and table look-up are substantial, and after tending together for some distance, they again tend to diverge.

The wall heat-transfer rate for the windward plane from the perfect gas prediction is about ten percent less than the table look-up results (Figure 8) and diverges downstream. The difference between the table look-up and Bade data is fairly small (within two percent).

The streamwise skin-friction coefficient shows results similar to the wall heat-transfer rate (Figure 9) data.

The transverse variation of wall pressure (Figure 10), wall heat-transfer rate (Figure 11), streamwise (Figure 12) and transverse (Figure 13) skin-friction coefficients show similar trends.

The variations in the force and moment data for one case are shown in Table 4. The inviscid axial and normal force coefficients for perfect gas conditions are four and twelve percent less than the table look-up results, while the viscous axial and normal force coefficients are nine and sixteen percent less. The variation of the center of pressure is about two percent. The differences between the table look-up and Bade results are much smaller and quite acceptable.

Case C ($\alpha = 10$ degrees)

The variation of wall pressure for the windward plane does not show the

divergence noted earlier, but substantial differences are observed in the nose region (Figure 14).

The streamwise skin-friction coefficient (Figure 15) shows good agreement for this case.

The transverse variation of wall pressure (Figure 16) shows large differences on the leeward side. Due to crossflow separation, data are not available up to the leeward plane. The differences in streamwise skin-friction coefficient are nearly constant in the transverse direction at a downstream section (Figure 17). The transverse variation of the transverse skin-friction coefficient is shown in Figure 18.

The force and moment data for this case are shown in Table 5. The differences between perfect gas and the table look-up results are much smaller. The axial force coefficient for perfect gas conditions is seven percent less than the table look-up results, while the center of pressure locations are within about one percent.

Case D ($\alpha = 20$ degrees)

The streamwise variations for all the quantities are similar to those for Case C. At the same section there is earlier crossflow separation due to the higher angle of attack.

The transverse variations of wall pressure (Figure 19), wall heat-transfer rate (Figure 20), streamwise (Figure 21) and transverse (Figure 22) skin-friction coefficients are also similar.

The axial force coefficient for perfect gas is six percent less than the table look-up results (Table 6), while the center of pressure location is nearly the same.

Computing Times Required

Computing times given in the tables are with the table look-up time as a reference of 100. Due to the absence of some input/output for the perfect gas model, the time for this condition is slightly lower than the Cohen and Bade options. If one omits the extra printout, the curve-fit of equilibrium properties and perfect gas computing times are very comparable and result in a sixty percent reduction in the computing time required for the table look-up model.

For low values of wall temperature, since all the equilibrium models essentially use Sutherland's viscosity and the density from the table look-up and Bade options is in good agreement, the differences in the wall heat-transfer rate are probably due to the differences in the Prandtl number.

CONCLUSIONS

In general, wall heat-transfer rate differences between the perfect gas and table look-up results are about ten percent, while the axial force coefficients differ by five to fifteen percent. Large pressure differences in the

nose region (which constitutes a significant percentage of the frontal area) probably cause the large differences in axial force.

Curve-fits can be effectively used to model the thermodynamic and transport properties of air in chemical equilibrium producing reasonably good force and moment coefficient predictions and with computing times that are comparable to the perfect gas model. The differences in wall heat-transfer rate for equilibrium flow are probably caused by the differences in Prandtl number.

Since there are considerable differences between the perfect gas and equilibrium air results, the viscous shock-layer method just developed should be used to predict viscous flows in chemical equilibrium, such as for reentry conditions, with good accuracy and within reasonable computing times.

NOMENCLATURE

| | |
|--------------|---|
| C_{f_s} | skin-friction coefficient in the streamwise direction |
| C_{f_ϕ} | skin-friction coefficient in the transverse direction |
| C_p | constant pressure specific heat |
| h | static enthalpy, h^*/U_∞^2 |
| H | total enthalpy, $h + (u^2 + v^2 + w^2)/2$ |
| k_t | eddy thermal conductivity, $-(\rho v) \overline{h'}/(\epsilon^2 \partial h/\partial n)$ |
| M | Mach number |
| n_{sh} | shock-standoff distance, n_{sh}^*/R^* |
| p | pressure, $p^*/\rho_\infty U_\infty^2$ |
| Pr | Prandtl number |
| Pr_t | turbulent Prandtl number, $C_p \mu_t/k_t$ |
| Q | convective heating rate, Btu/ft ² -sec |
| r | distance from and normal to the body axis, r^*/R^* |
| R^* | body nose radius |
| s, n, ϕ | general surface-normal coordinate system streamwise, normal and crossflow directions |
| T | temperature |
| T_{ref}^* | reference temperature, U_∞^2/C_p^* |

u, v, w streamwise, normal and crossflow velocity components nondimensionalized by the freestream velocity, U_∞^*
 W dependent variable
 α angle of attack
 γ ratio of specific heat
 ϵ Reynolds number parameter, $\epsilon^2 = \mu_{ref}^* / \rho_\infty U_\infty R^*$
 ϵ^+ μ_t / μ
 θ body angle in the streamwise direction
 μ viscosity, μ^* / μ_{ref}^*
 μ_{ref}^* reference viscosity, $\mu^*(T_{ref})$
 μ_t eddy viscosity, $-(\rho v)'u' / (\epsilon^2 \partial u / \partial n)$
 ρ density, ρ^* / ρ_∞

Subscripts

B Bade
 C Cohen
 INV Inviscid
 s Streamwise
 sh conditions behind the bow shock wave
 t turbulent quantity
 w wall condition
 ∞ dimensional freestream conditions
 ϕ transverse

Superscripts

$*$ dimensional quantity
 $'$ fluctuating value

REFERENCE

1. Miner, E. W., Anderson, E. C. and Lewis, C. H.: "A Computer Program for Two Dimensional and Axisymmetric Nonreacting Perfect Gas and Equilibrium Chemically Reacting Laminar Transitional and/or Turbulent Boundary-Layer Flows," VPI-E-71-8, May 1971.
2. Cohen, N. B.: "Correlation Formulas and Tables of Density and Some Thermodynamic Properties of Equilibrium Dissociating Air for Use in Solutions of the Boundary-Layer Equations," NASA TN D-194, February 1960.
3. Lubard, S. C. and Helliwell, W. S.: "Calculation of the Flow on a Cone at High Angle of Attack," AIAA J., Vol. 12, July 1974, pp. 965-974.
4. Murray, A. L. and Lewis, C. H.: "Hypersonic Three-Dimensional Viscous Shock-Layer Flow over Blunt Bodies," AIAA J., Vol. 16, No. 12, pp. 1279-1286, December 1978.
5. Szema, K. Y. and Lewis, C. H.: "Three-Dimensional Hypersonic Laminar, Transitional and/or Turbulent Shock-Layer Flows," AIAA Paper No. 80-1457, July 1980.
6. Cebeci, T.: "Behavior of Turbulent Flows near a Porous Wall with Pressure Gradient," AIAA J., Vol. 8, No. 12, pp. 2152-2156, December 1970.
7. Dhawan, S. and Narasimha, R.: "Some Properties of Boundary Layer Flow During the Transition from Laminar to Turbulent Motion," Journal of Fluid Mechanics, Vol. 3, pt. 4, pp. 418-436, January 1958.
8. Hansen, C. F.: "Approximations for the Thermodynamic and Transport Properties of High Temperature Air," NASA TR R-50, 1959.
9. Cebeci, T. and Smith, M. O.: Analysis of Turbulent Boundary Layers, Academic Press, 1974.
10. Anderson, C., Moss, J. N. and Sutton, K.: "Turbulent Viscous Shock-Layer Solutions with Strong Vorticity Interaction," AIAA Paper No. 76-120, January 1976.
11. Klebanoff, P. S.: "Characteristics of Turbulence in a Boundary Layer with Zero Pressure Gradient," NASA Report 1247, 1955.
12. Clauser, F. H.: "The Turbulent Boundary Layer," Advances in Applied Mechanics, H. L. Dryden and Th. von Karman, Eds., Academic Press, 1956, pp. 1-15.
13. White, F. M.: Viscous Fluid Flow, McGraw-Hill Book Company, 1974.
14. Lordi, J. A., Mates, R. E. and Moselle, J. R.: "A Computer Program for the Numerical Solution of Non-equilibrium Expansions of Reacting Gas Mixtures," CAL RPT No. AD-K89-A-6, 1965.
15. Moeckel, W. E. and Weston, K. C.: "Composition and Thermodynamic Properties of Air in Chemical Equilibrium," NACA TN 4265, 1958.

16. Bade, W. L.: "Simple Analytical Approximation to the Equation of State of Dissociating Air," ARS Journal, Vol. 29, No. 4, April 1959.
17. Davis, R. T.: "Numerical Solution of the Hypersonic Viscous Shock Layer Equations," AIAA J., Vol. 8, No. 5, pp. 843-851, May 1970.
18. Frieders, M. C. and Lewis, C. H.: "Effects of Mass Transfer into Laminar and Turbulent Boundary Layers over Cones at Angle of Attack," VPI-AERO-031, March 1975.

TABLE 1. Freestream Conditions

| | | | |
|--|----------|----------|----------|
| Altitude, h (feet) | 40,000 | 80,000 | 160,000 |
| M_∞ | 20.6 | 20.4 | 18.4 |
| Velocity, U_∞ (ft/sec) | 20,000 | 20,000 | 20,000 |
| Pressure, p_∞ (lb/ft ²) | 393.085 | 58.505 | 1.942 |
| Temperature, T_∞ (R) | 389.97 | 397.69 | 487.17 |
| Density, ρ_∞ (slug/ft ³) | 5.873E-4 | 8.571E-5 | 2.322E-6 |
| Reynolds Number (per foot) | 3.955E7 | 5.679E6 | 1.305E5 |

TABLE 2. Test Cases

| Case | α (degrees) | Alt (feet) | T_w (R) | T_w/T_∞ | Flow |
|------|-----------------------|---------------|--------------|----------------|-----------|
| A | 0 | 80,000 | 540 | 1.36 | Laminar |
| B | 2 | 40,000 | 3600 | 9.16 | Turbulent |
| C | 10 | 80,000 | Adiabatic | - | Laminar |
| D | 20 | 80,000 | 540 | 1.36 | Laminar |

TABLE 3. Force and Moment Data (Case A)

$\alpha = 3$ deg, Alt = 80,000 feet, $T_w = 540R$, S/R = 30

| | Actual Values | | | |
|----------------|--------------------------------|----------|----------|----------|
| | PG | TLU | COHEN | BADE |
| $C_{A_{INV}}$ | 0.070216 | 0.076465 | 0.076465 | 0.076465 |
| C_{A_P} | 0.06831 | 0.07538 | 0.07509 | 0.07557 |
| $C_{A_{SF}}$ | 0.00251 | 0.00245 | 0.00209 | 0.00218 |
| $C_{A_{TOT}}$ | 0.070824 | 0.077835 | 0.077176 | 0.077757 |
| TIME* (Sec) | 72 | 233 | 102 | 100 |
| | Percent Variation Based on TLU | | | |
| | PG | COHEN | BADE | |
| $C_{A_{INV}}$ | 8.2 | 0.0 | 0.0 | |
| C_{A_P} | 9.4 | 0.4 | -0.3 | |
| $C_{A_{SF}}$ | -2.4 | 14.7 | 11.0 | |
| $C_{A_{TOT}}$ | 9.0 | 0.8 | 0.1 | |
| TIME† | 33 | 44 | 43 | |

* IBM 370/3032 with FORTHX COMPILER (OPT2)

† Based on TLU=100

TABLE 4. Force and Moment Data (Case B)

$\alpha = 2$ deg, Alt = 40,000 feet, $T_w = 3600^{\circ}\text{R}$ S/R = 32

| | Actual Values | | | Percent Variation Based on TLU | |
|---------------|---------------|-----------|-----------|-----------------------------------|-----------------|
| | PG | TLU | BADE | PG | BADE |
| $C_{A_{INV}}$ | 0.06331120 | 0.0654952 | 0.0654952 | 3.3 | 0.0 |
| $C_{N_{INV}}$ | 0.0345556 | 0.0392156 | 0.0392156 | 11.9 | 0.0 |
| C_A | 0.071163 | 0.078564 | 0.078414 | 9.4 | 0.2 |
| C_N | 0.032386 | 0.038607 | 0.038653 | 16.1 | -0.1 |
| C_M | -0.021207 | -0.025800 | -0.025856 | 17.8 | -0.2 |
| Z_{cp}/L | 0.654814 | 0.668288 | 0.668924 | 2.0 | -0.1 |
| $C_{A_{SF}}$ | 0.00595 | 0.00744 | 0.00710 | 20.0 | 4.6 |
| C_{A_P} | 0.06521 | 0.07112 | 0.07132 | 8.3 | -0.3 |
| TIME | 1778* | 5203* | 2384* | 34 [†] | 46 [†] |

* Seconds, IBM 370/3032 with FORTHX COMPILER (OPT2)

[†] Based on TLU=100

TABLE 5. Force and Moment Data (Case C)

$\alpha = 10$ deg, Alt = 80,000 ft, $T_w =$ Adiabatic, S/R = 32

| | Actual Values | | Percent Variation Based on TLU PG |
|---------------|---------------|-----------|---|
| | PG | TLU | |
| $C_{A_{INV}}$ | 0.094359 | 0.097347 | 3.1 |
| $C_{N_{INV}}$ | 0.296715 | 0.302710 | 2.0 |
| C_A | 0.099410 | 0.106954 | 7.1 |
| C_N | 0.302246 | 0.299984 | -0.8 |
| C_M | -0.198296 | -0.194445 | -2.0 |
| Z_{cp}/L | 0.656076 | 0.648185 | -1.2 |
| $C_{A_{SF}}$ | 0.00433 | 0.00482 | 10.2 |
| C_{A_P} | 0.09508 | 0.10214 | 6.9 |

TABLE 6. Force and Moment Data (Case D)

$\alpha = 20$ deg, Alt = 80,000 ft, $T_w = 540R$, S/R = 32

| | Actual Values | | Percent Variation Based on TLU PG |
|---------------|---------------|-----------|---|
| | PG | TLU | |
| $C_{A_{INV}}$ | 0.151591 | 0.155653 | 2.6 |
| $C_{N_{INV}}$ | 0.716164 | 0.727595 | 1.6 |
| C_A | 0.159610 | 0.170116 | 6.2 |
| C_N | 0.719390 | 0.732410 | 1.8 |
| C_M | -0.450558 | -0.459907 | 2.0 |
| Z_{CP}/L | 0.626305 | 0.627937 | 0.3 |
| $C_{A_{SF}}$ | 0.00613 | 0.00644 | 4.8 |
| C_{A_P} | 0.15348 | 0.16368 | 6.2 |

$\theta_c = 7$ degrees

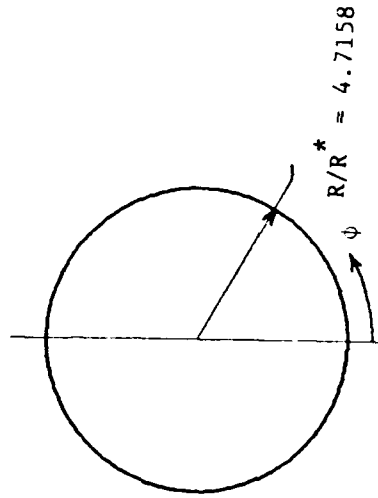
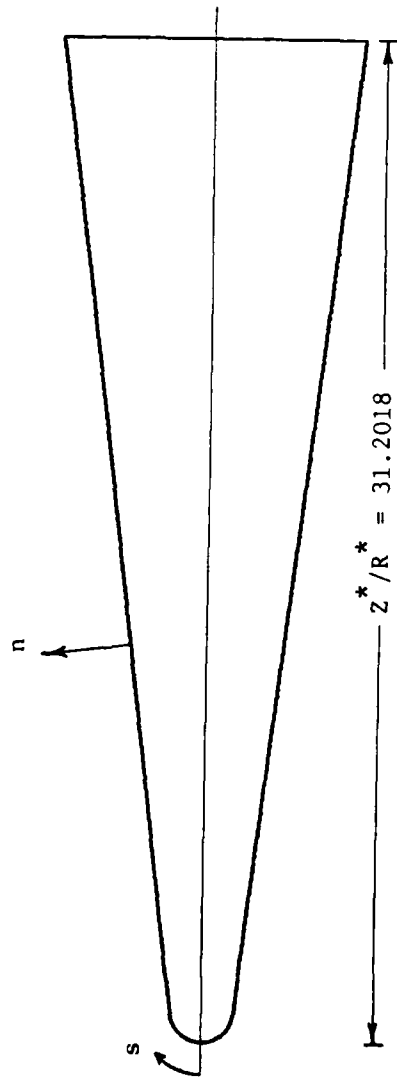


Figure 1. Non-Dimensional Body Geometry and Coordinate System

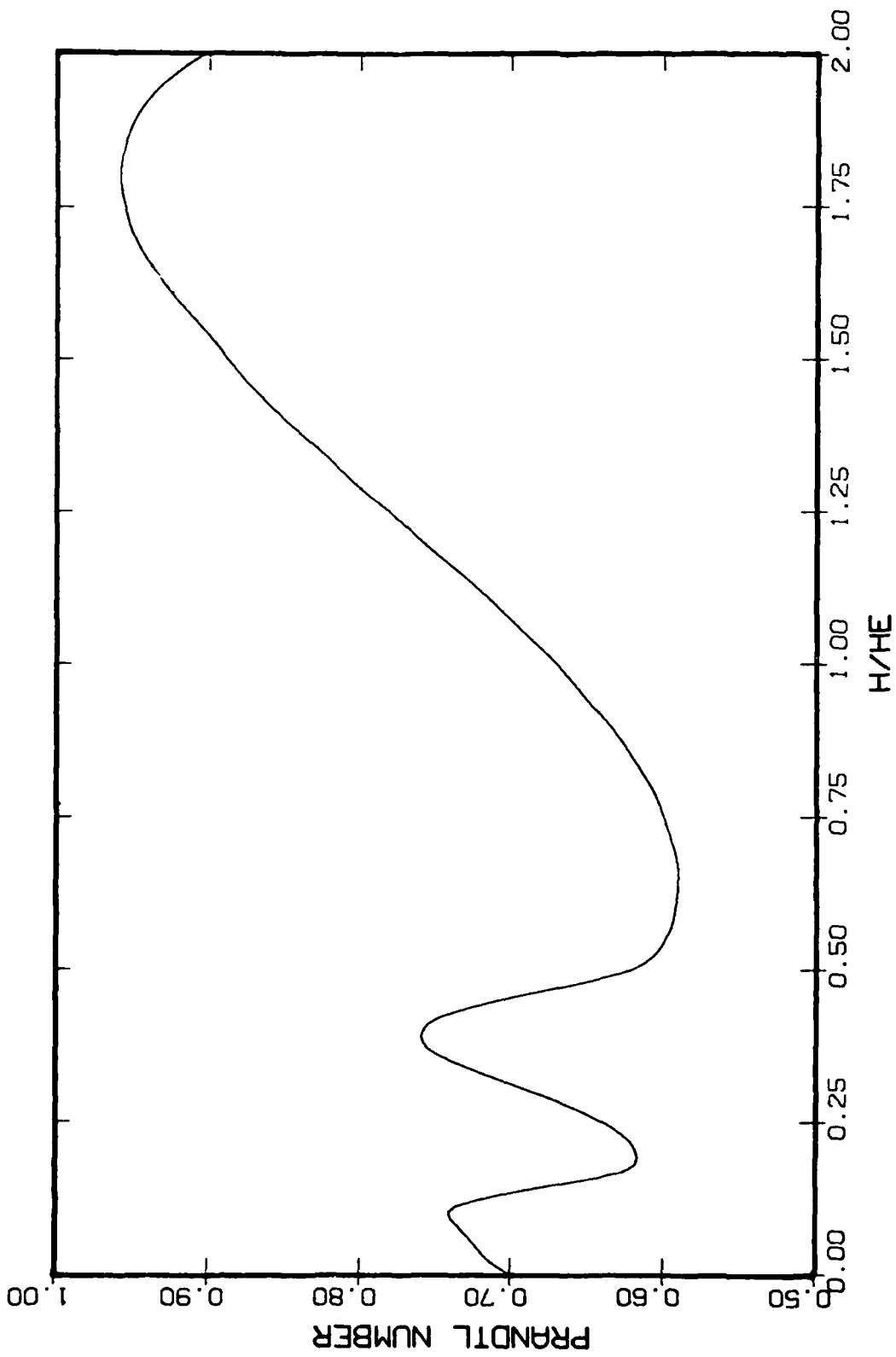


Figure 2. Prandtl Number Variation with Enthalpy Ratio (Cohen and Bade Options)

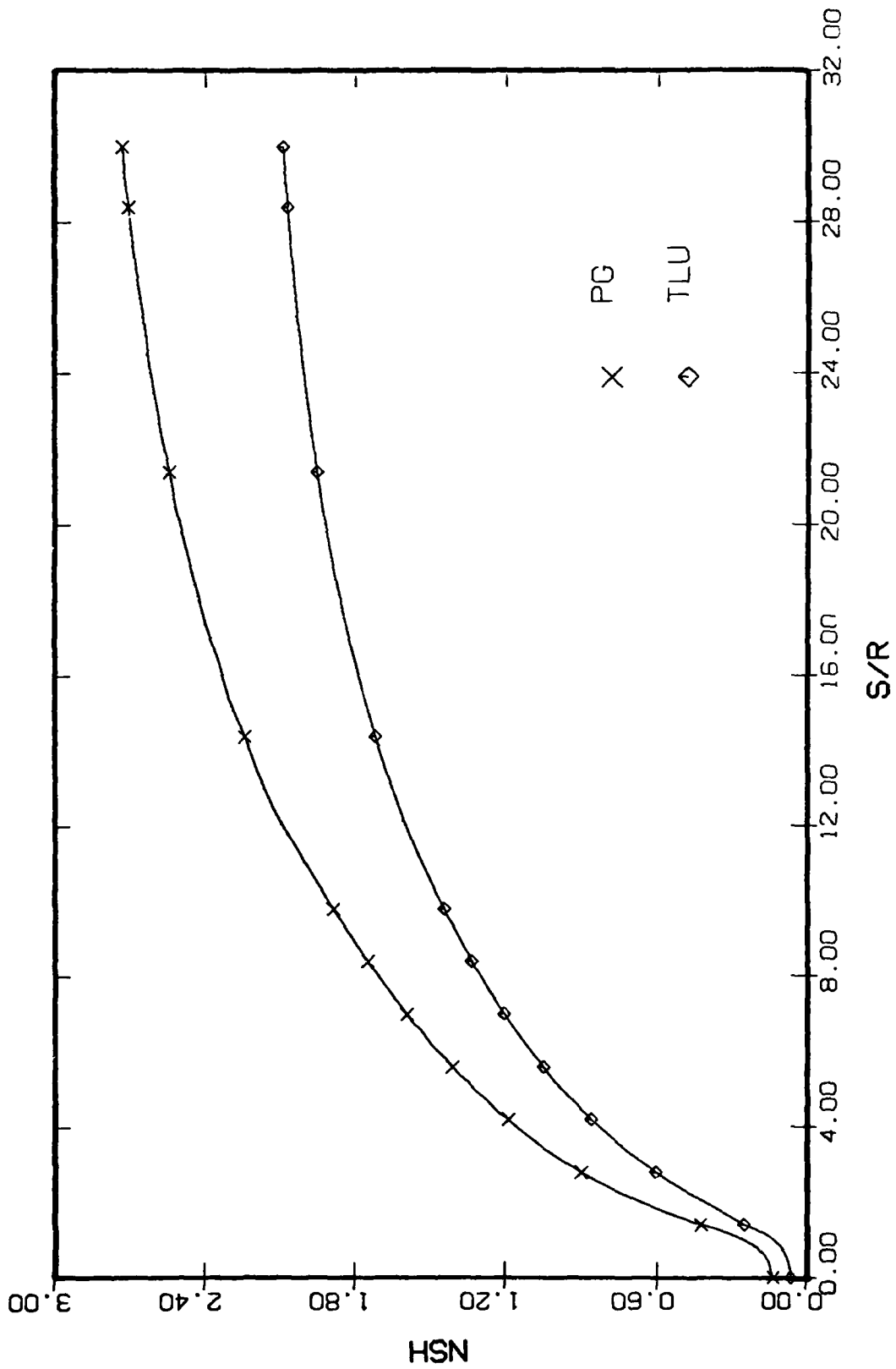


Figure 3. Streamwise Variation of Shock Standoff Distance (Case A, $\alpha = 0$ deg, Alt = 160,000 ft, $T_w = 3600R$)

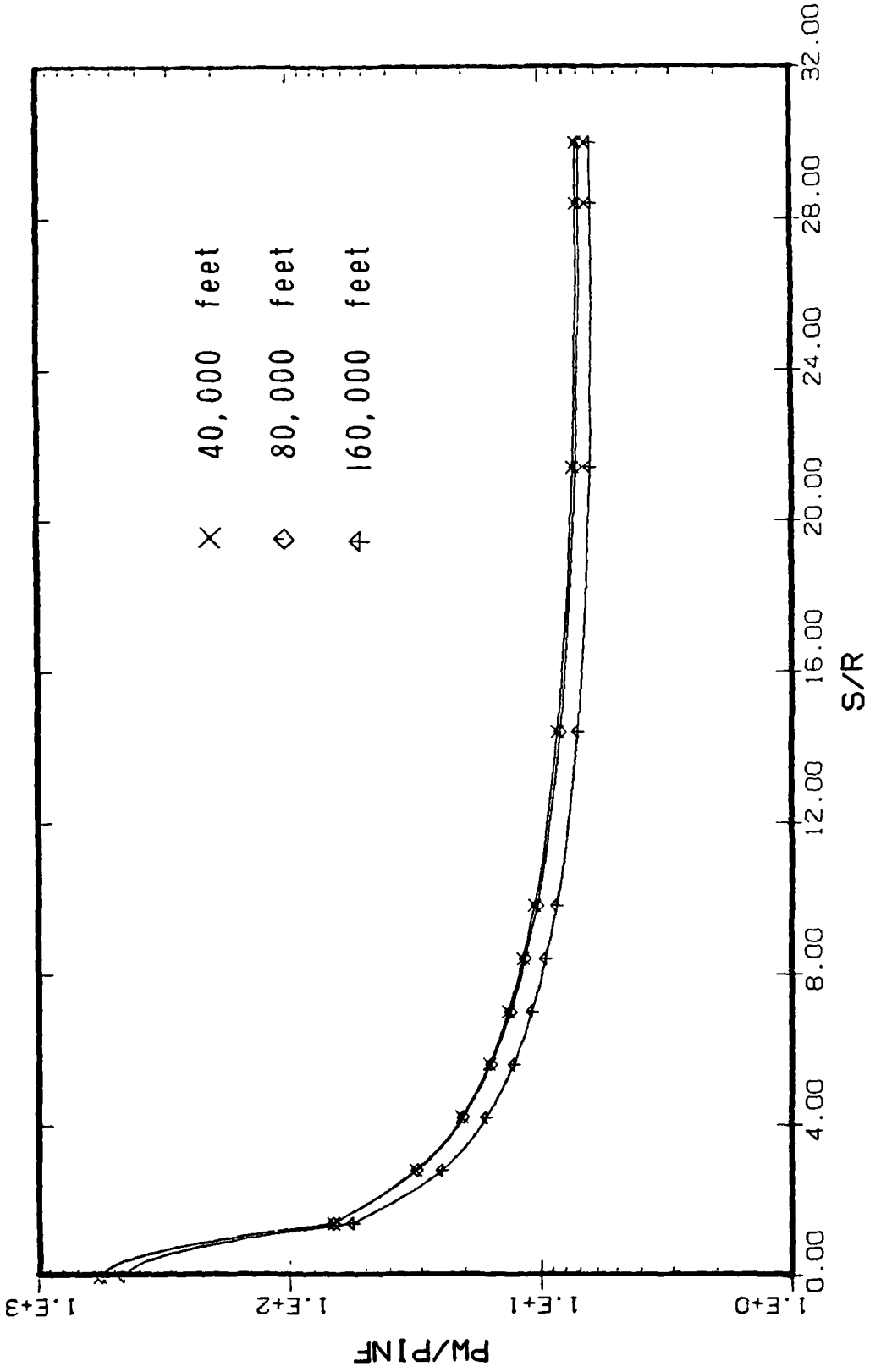


Figure 4. Streamwise Variation of Wall Pressure (Case A, $\alpha = 0$ deg, Alt = 40,000, 80,000 and 160,000 ft, $T_w = 540R$)

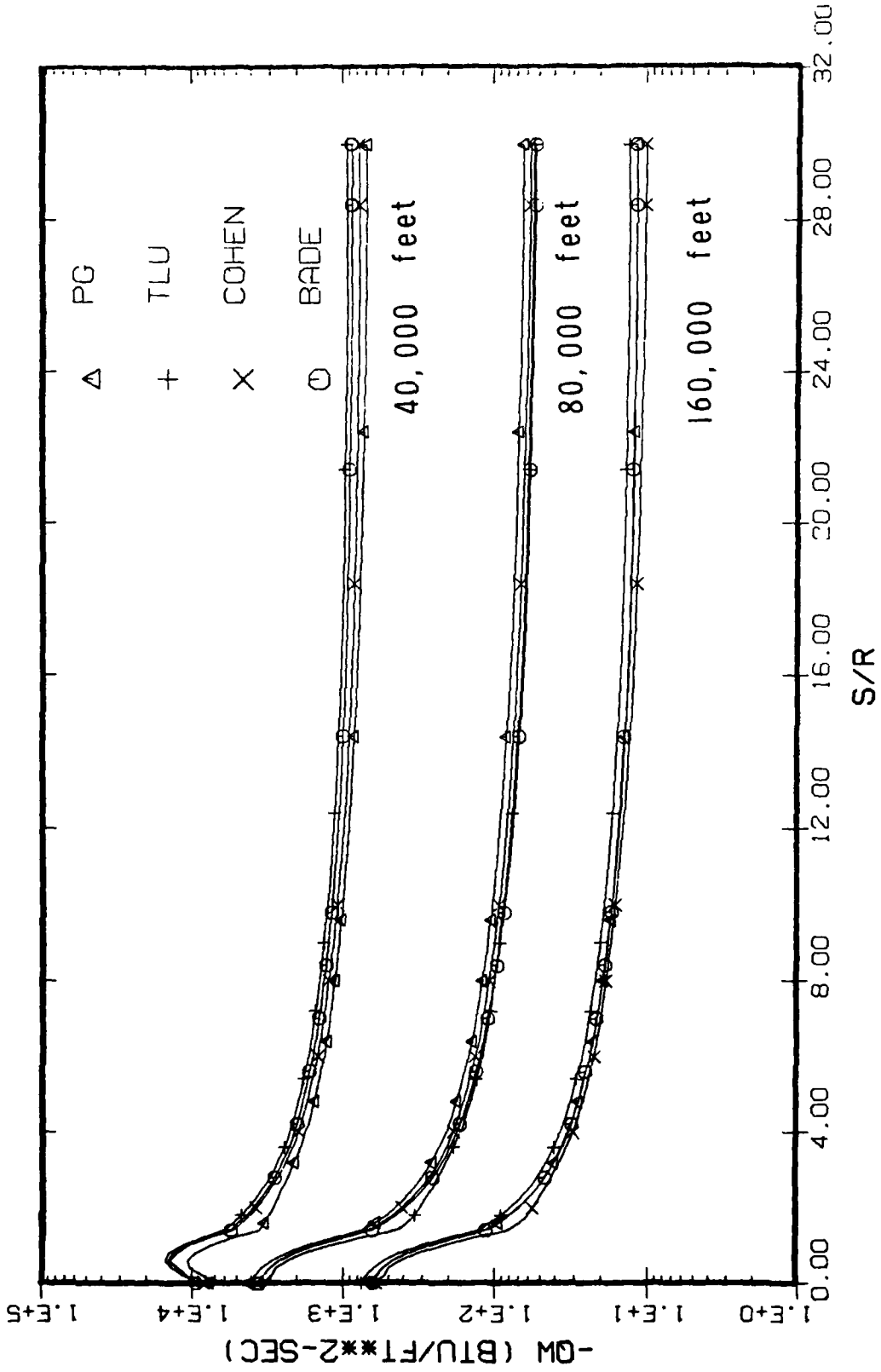


Figure 5. Streamwise Variation of Wall Heat-Transfer Rate (Case A, $\alpha = 0$ deg, Alt = 40,000, 80,000 and 160,000 ft, $T_w = 540R$)

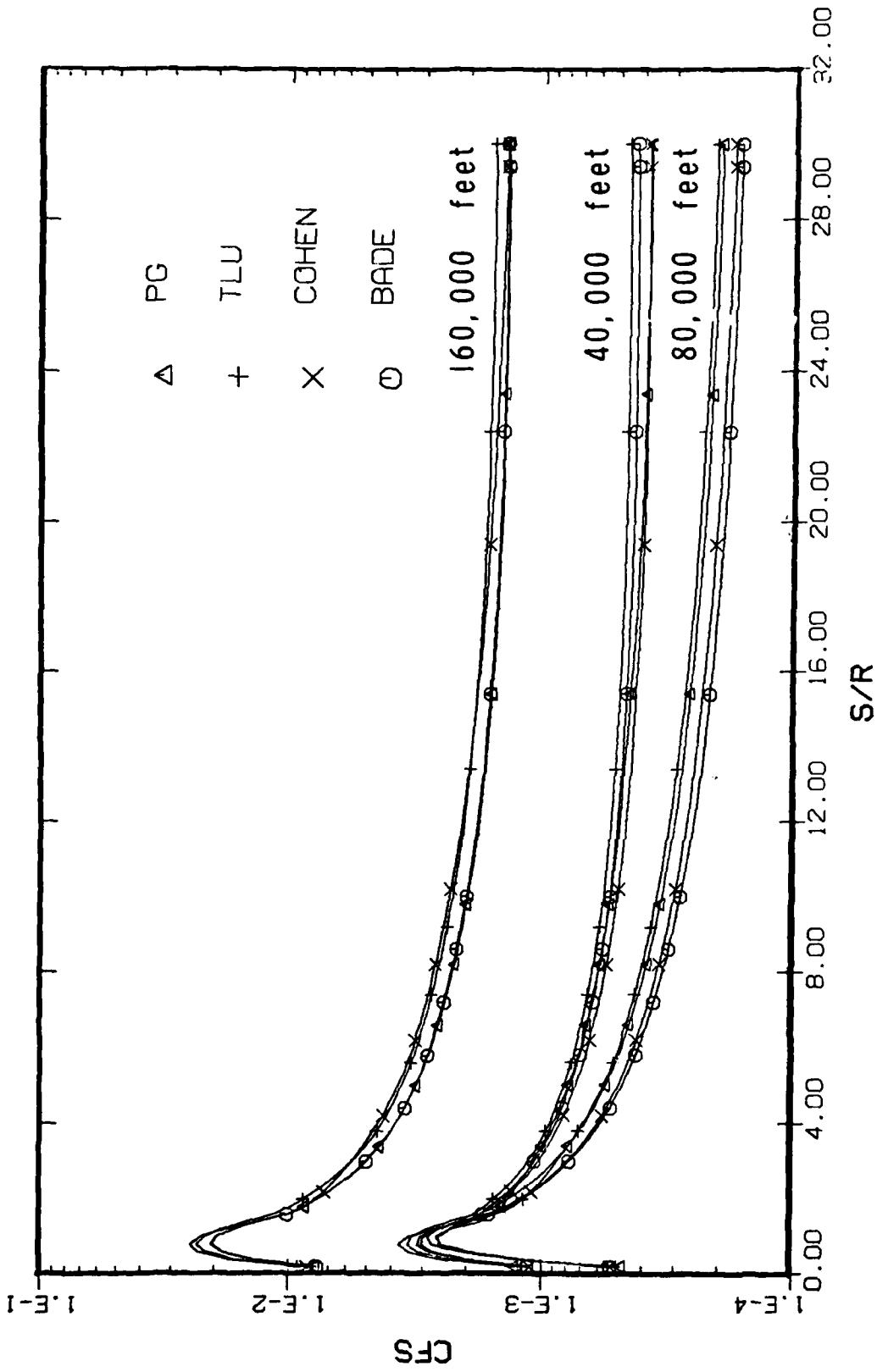


Figure 6. Streamwise Variation of C_{fs} (Case A, $\alpha = 0$ deg, Alt = 40,000, 80,000 and 160,000 ft, $T_w = 540R$)

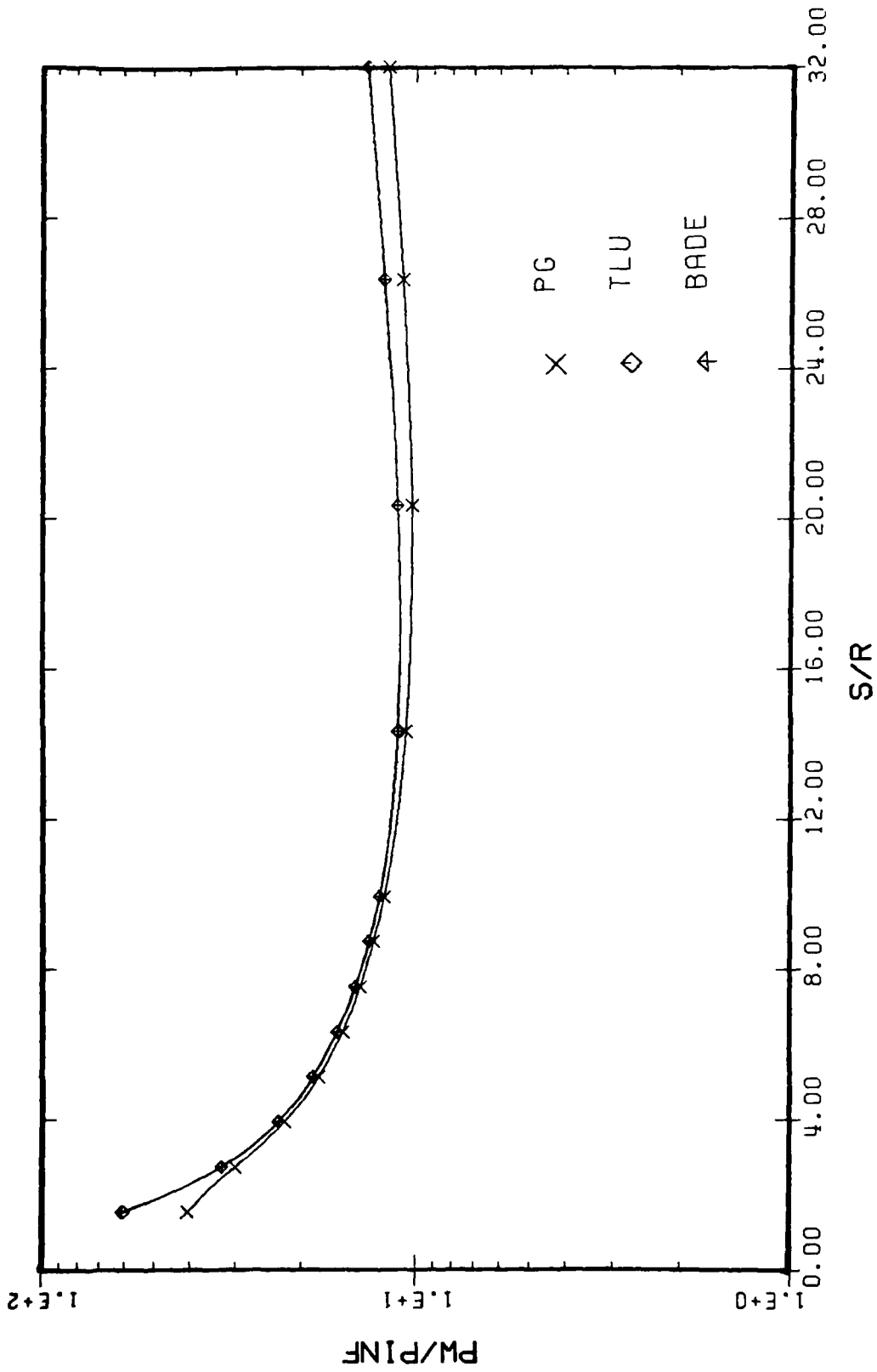


Figure 7. Streamwise Variation of Wall Pressure for $\phi = 0$ Plane
 (Case B, $\alpha = 2$ deg, Alt = 40,000 ft, $T_w = 3600R$)

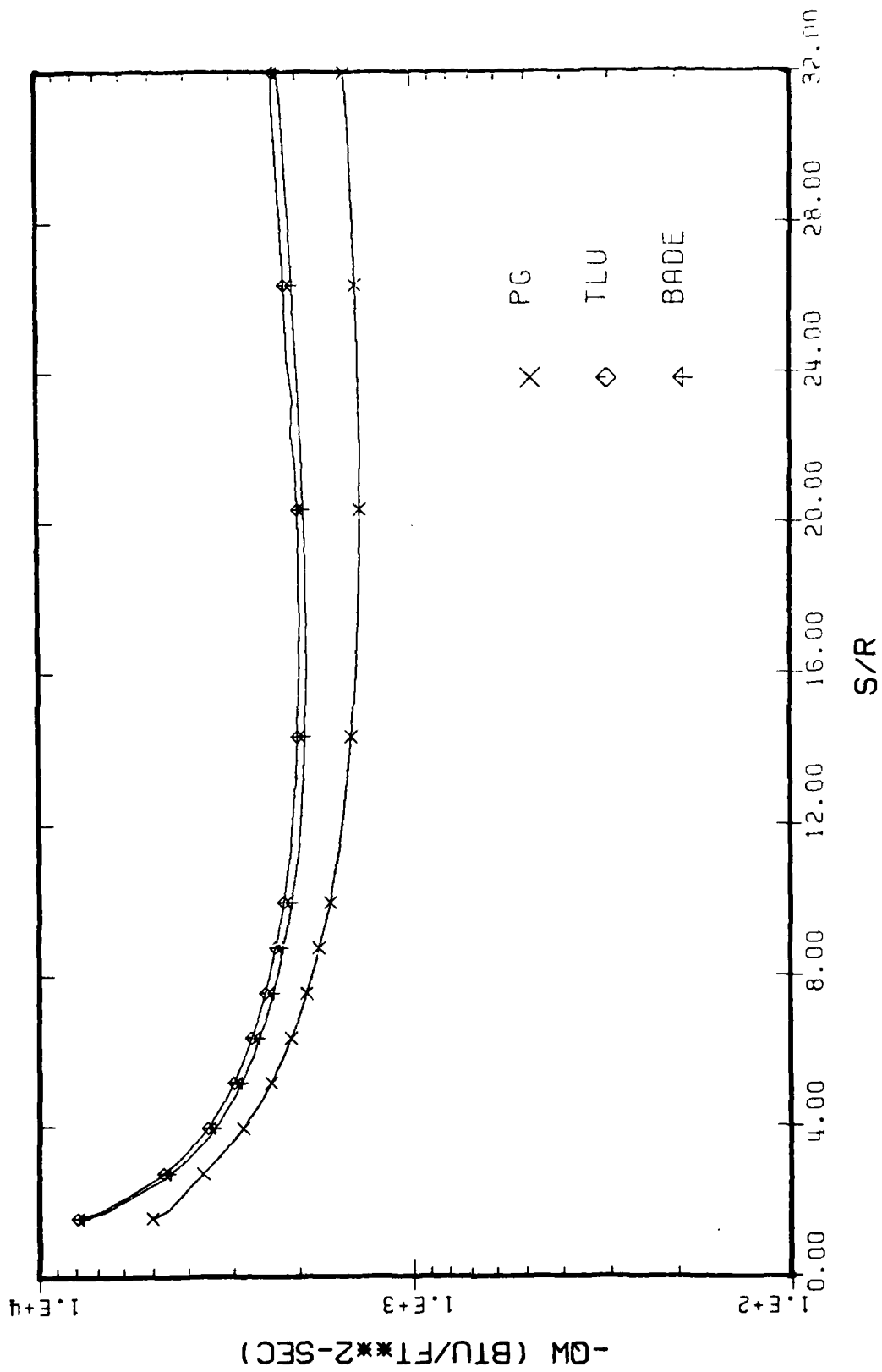


Figure 8. Streamwise Variation of Wall Heat-Transfer Rate for $\phi = 0$ Plane
 (Case B, $\alpha = 2$ deg, Alt = 40,000 ft, $T_w = 3600R$)

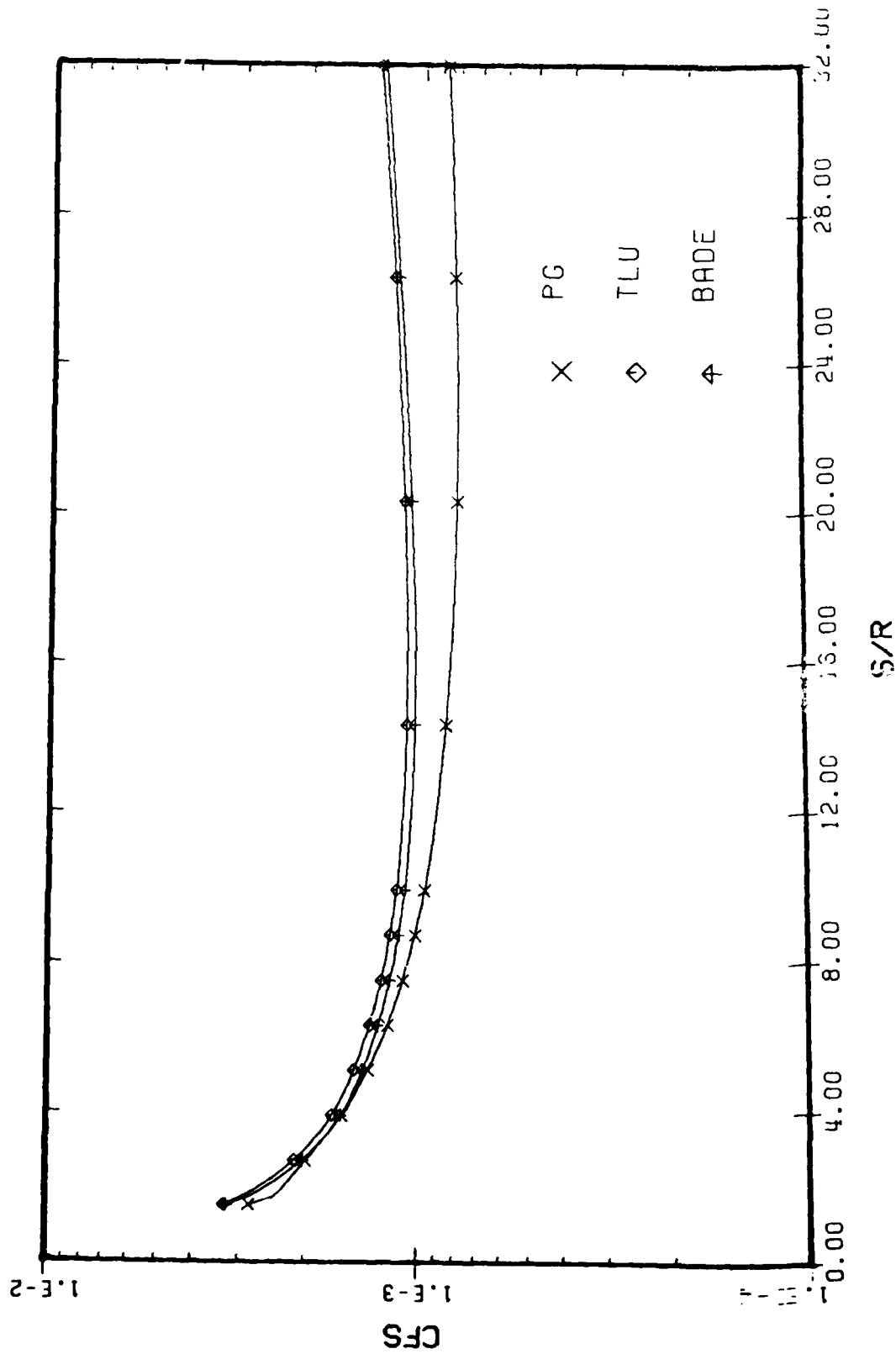


Figure 9. Streamwise Variation of C_{f_s} for $\phi = 0$ Plane (Case B,
 $\alpha = 2$ deg, Alt = 40,000 ft, $T_w = 3600R$)

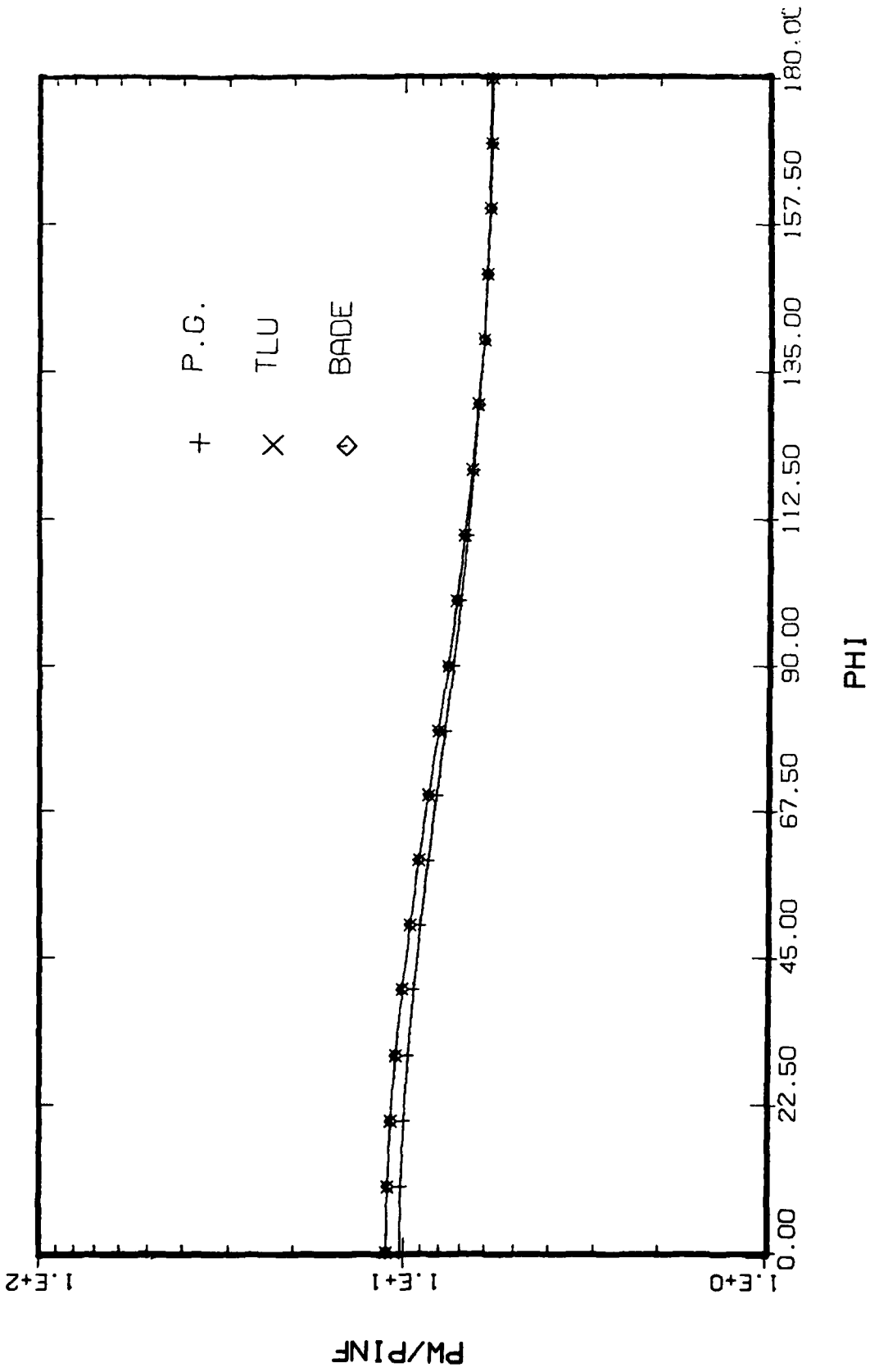


Figure 10. Transverse Variation of Wall Pressure at $S/R = 20$
 (Case B, $\alpha = 2$ deg, Alt = 40,000 ft, $T_w = 3600R$)

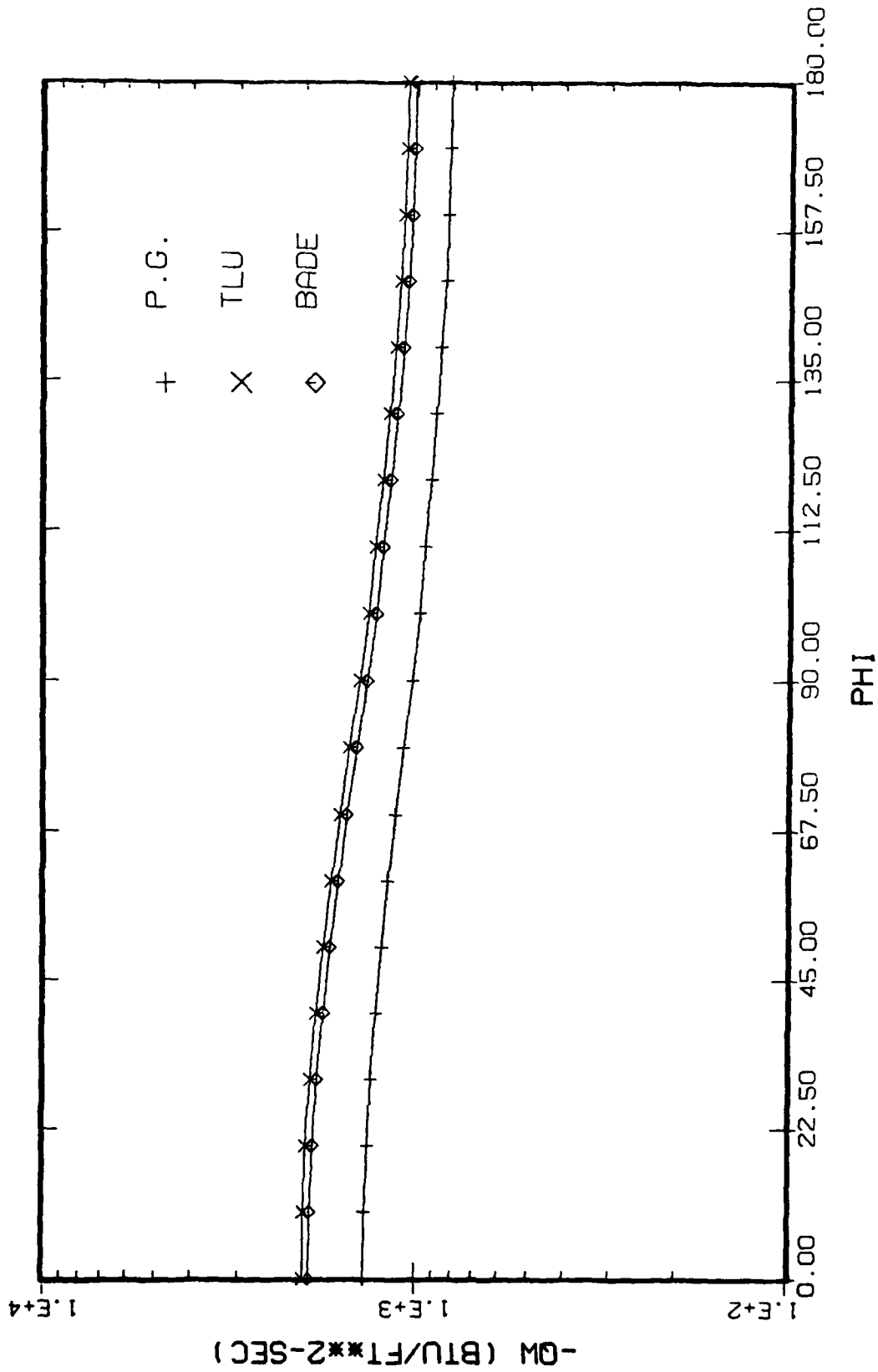


Figure 11. Transverse Variation of Wall Heat-Transfer Rate at S/R = 20
 (Case B, $\alpha = 2$ deg, Alt = 40,000 ft, $T_w = 3600R$)

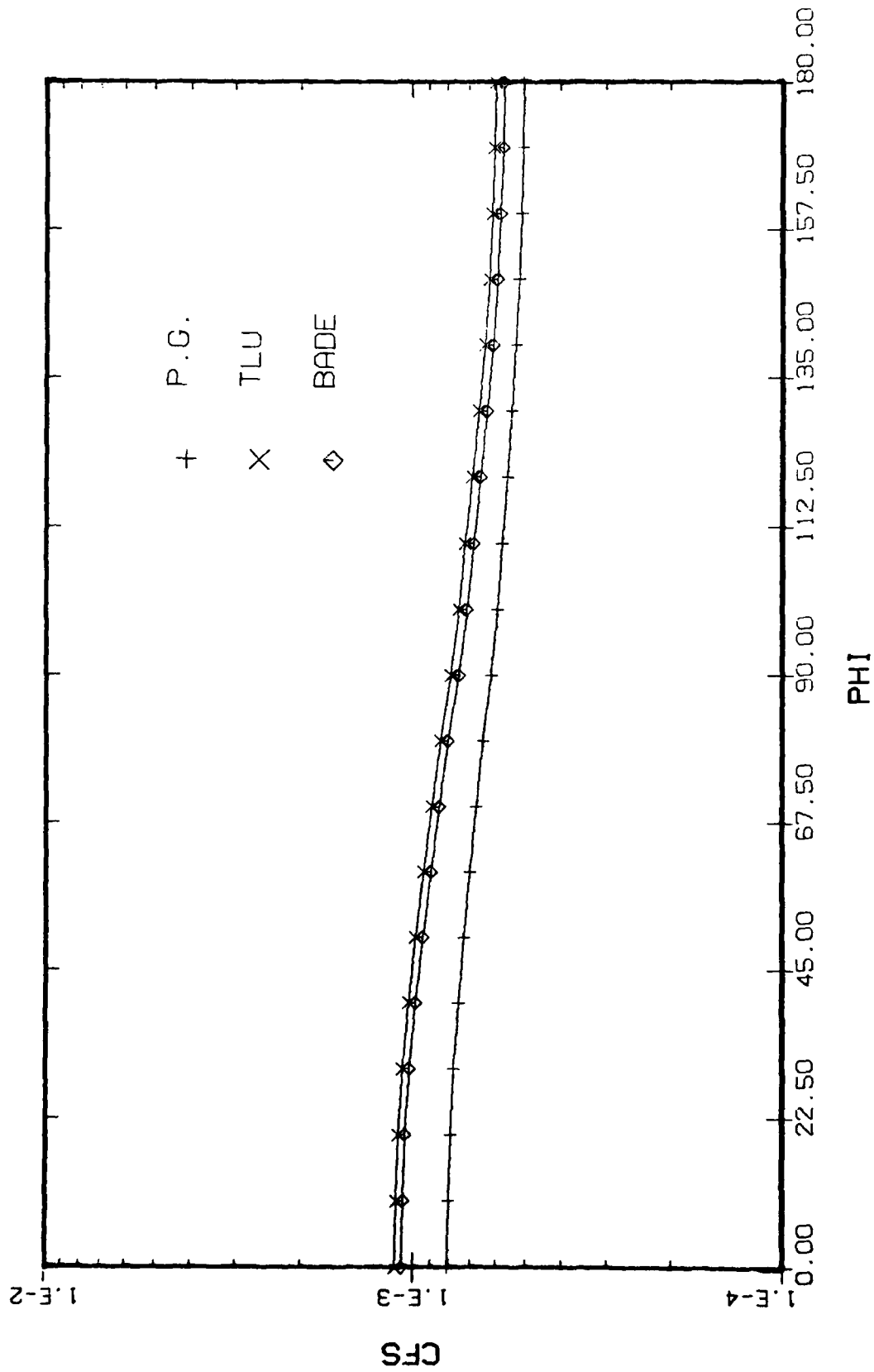


Figure 12. Transverse Variation of C_{fs} at $S/R = 20$
 (Case B, $\alpha = 2$ deg, Alt = 40,000 ft, $T_w = 3600R$)

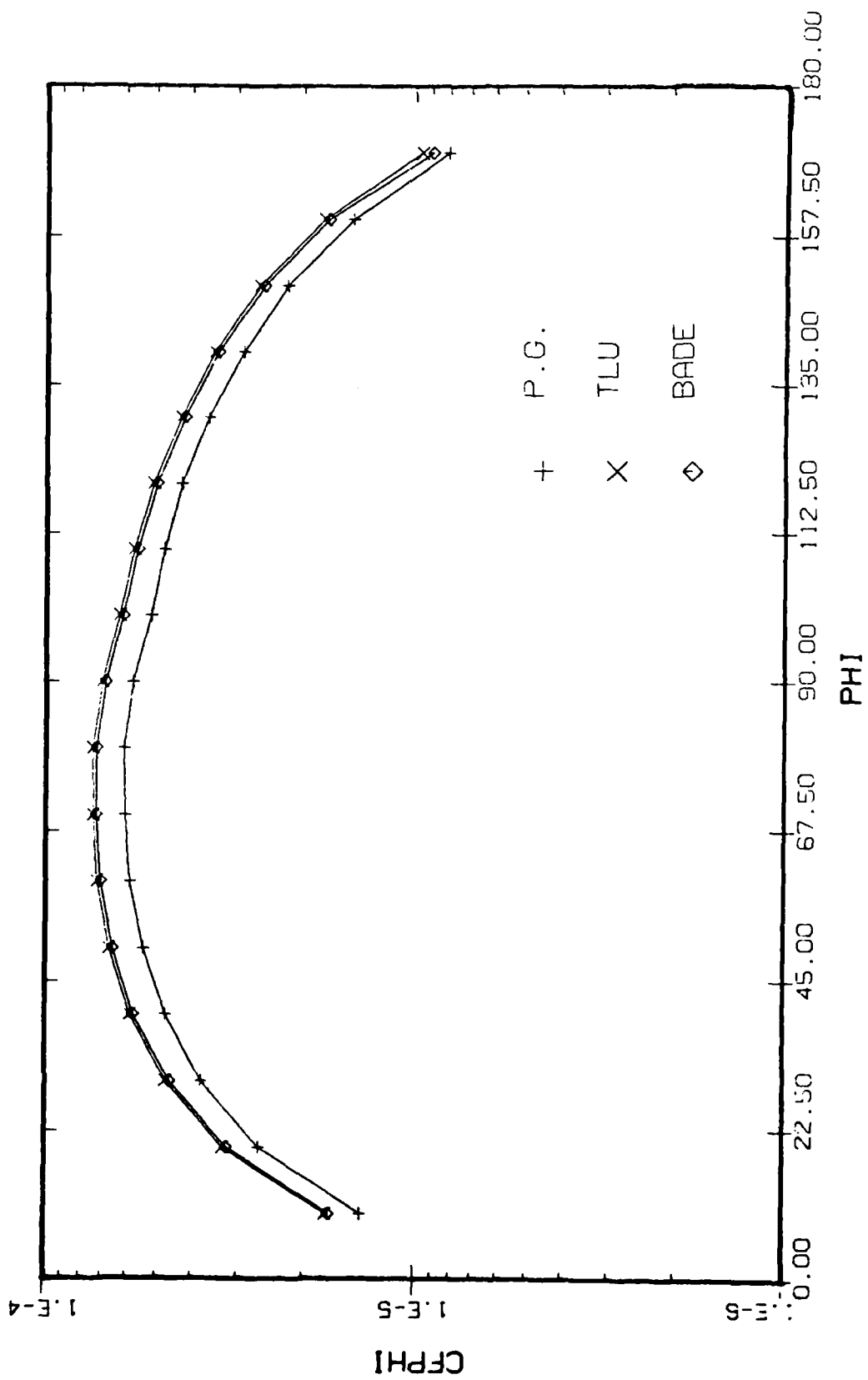


Figure 13. Transverse Variation of $C_{f\phi}$ at $S/R = 20$
 (Case B, $\alpha = 2$ deg, Alt = 40,000 ft, $T_w = 3600R$)

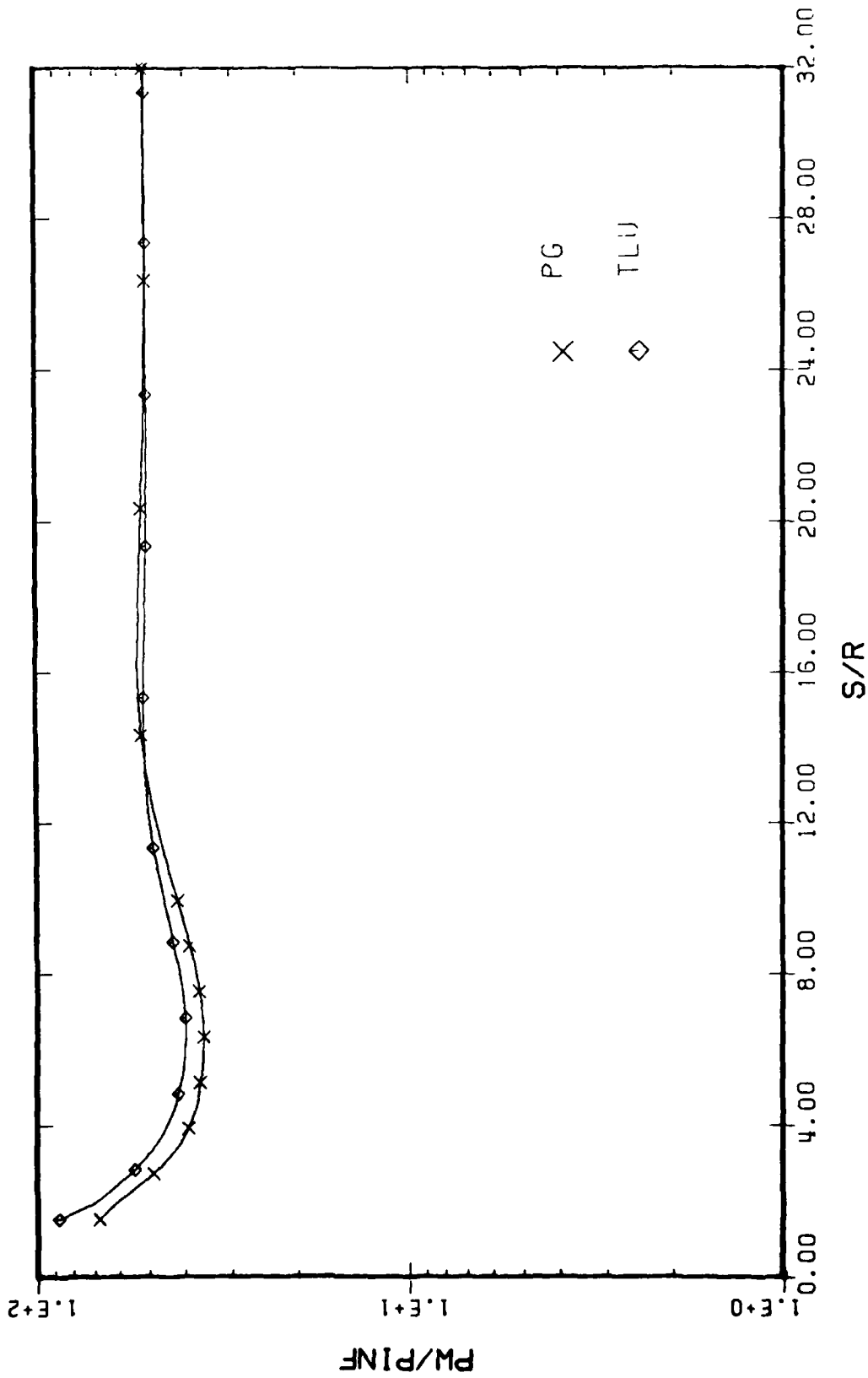


Figure 14. Streamwise Variation of Wall Pressure for $\phi = 0$ Plane
 (Case C, $\alpha = 10$ deg, Alt = 80,000 ft, $T_w = \text{Adiabatic}$)

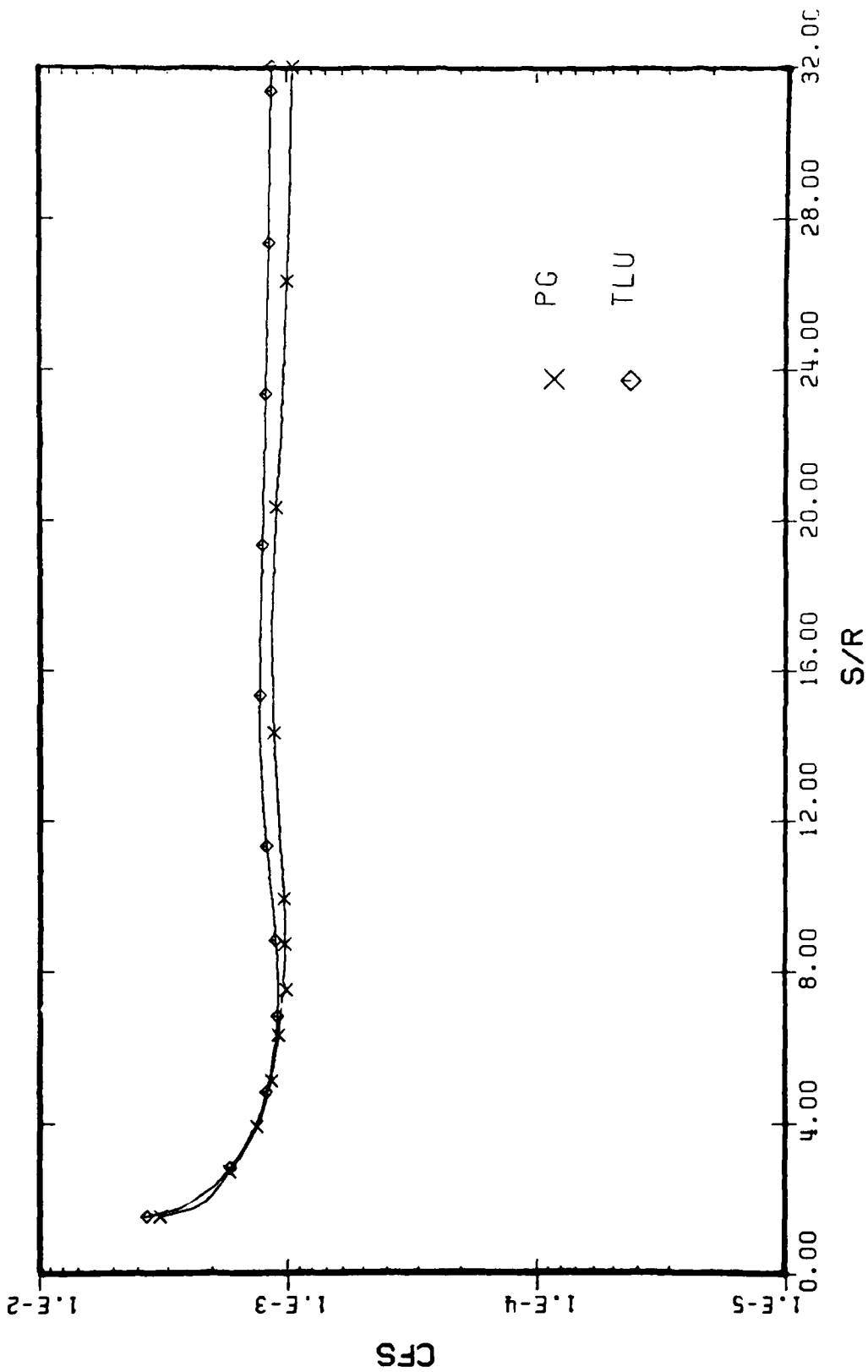


Figure 15. Streamwise Variation of C_{f_s} for $\phi = 0$ Plane
 (Case C, $\alpha = 10$ deg, Alt = 80,000 ft, $T_w = \text{Adiabatic}$)

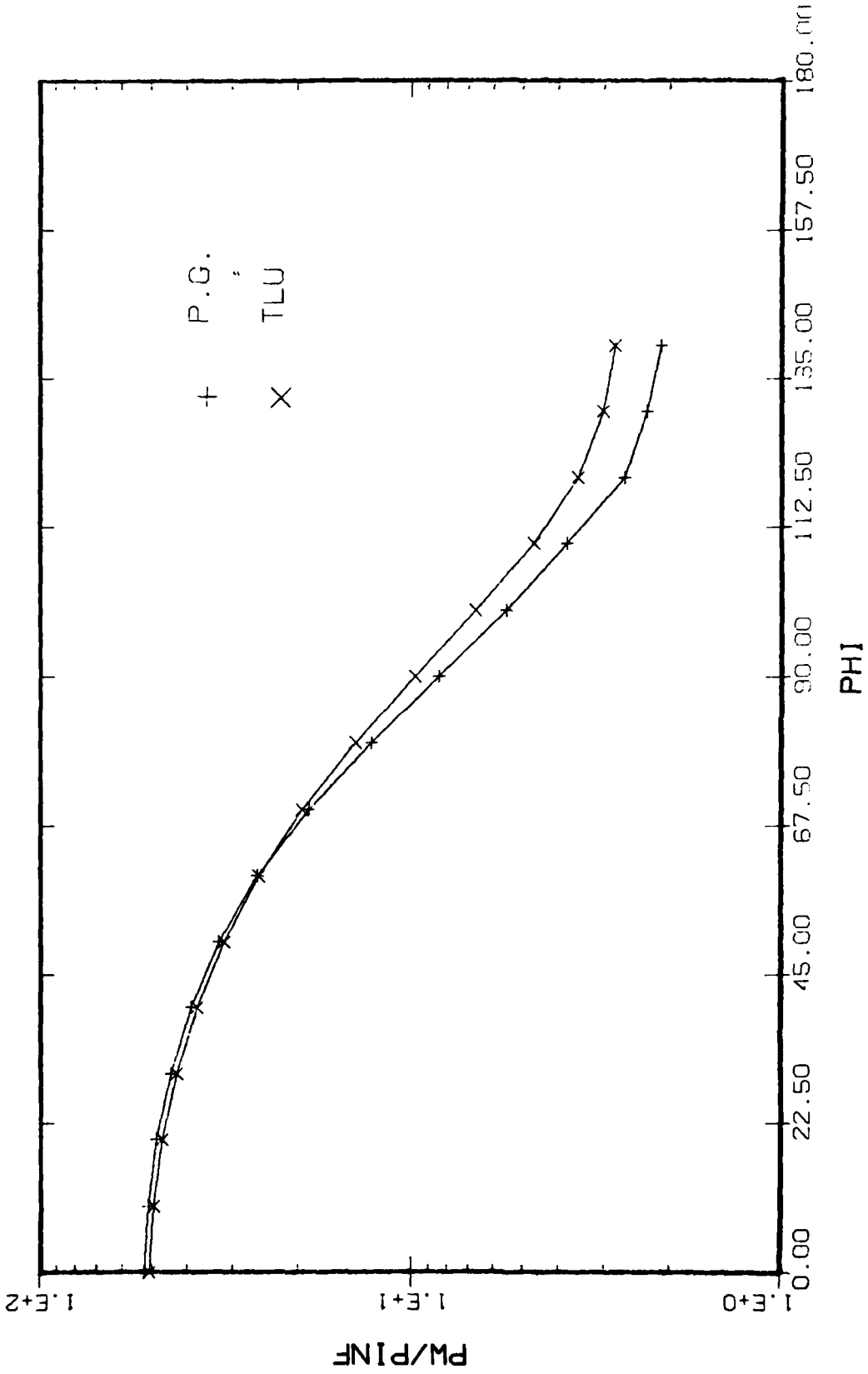


Figure 16. Transverse Variation of Wall Pressure at $S/R = 20$
 (Case C, $\alpha = 10$ deg, Alt = 80,000 ft, $T_w = \text{Adiabatic}$)

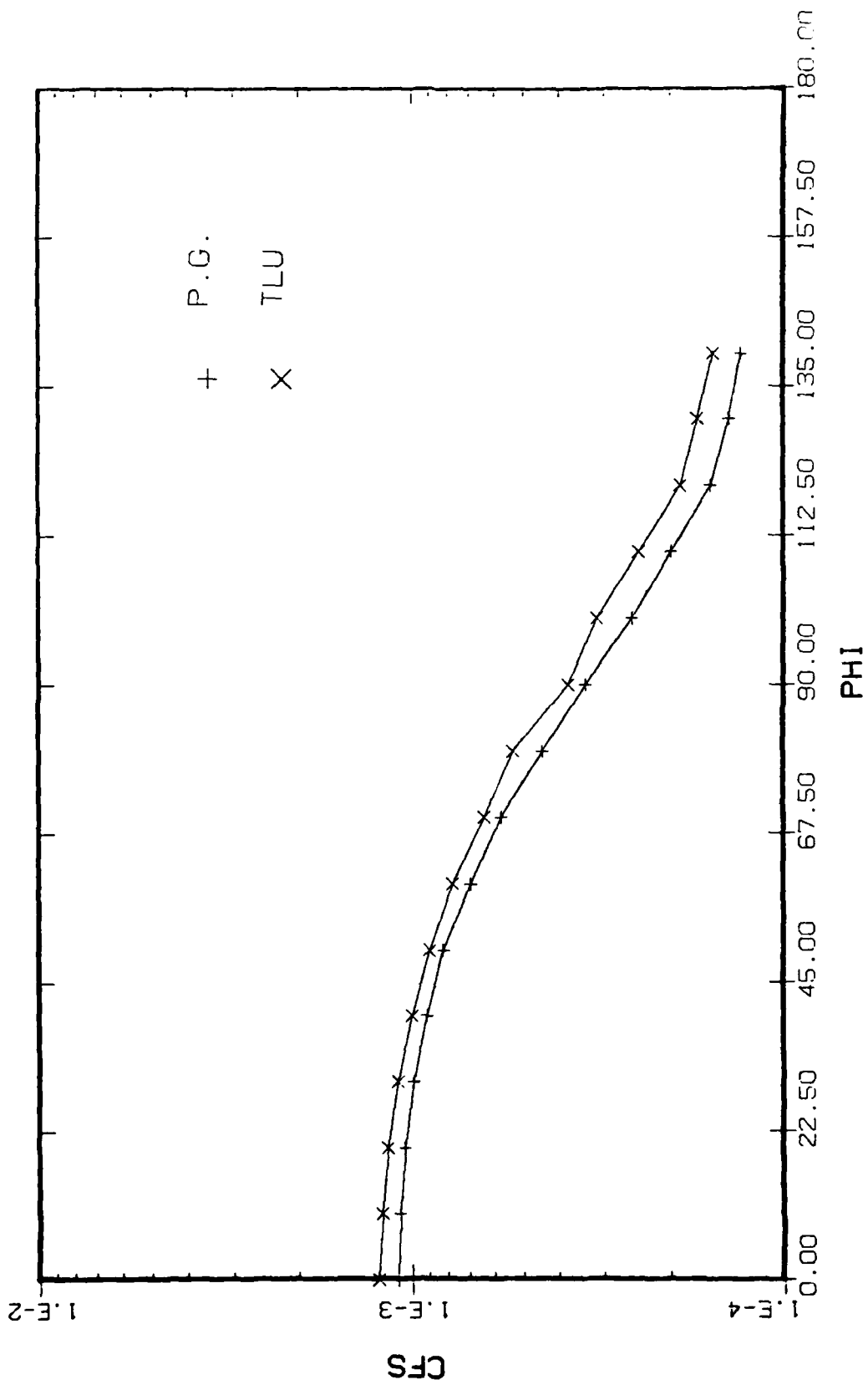


Figure 17. Transverse Variation of Cf_r at $S/R = 20$
 (Case C, $\alpha = 10$ deg, Alt = 80,000 ft, $T_w = \text{Adiabatic}(r)$)

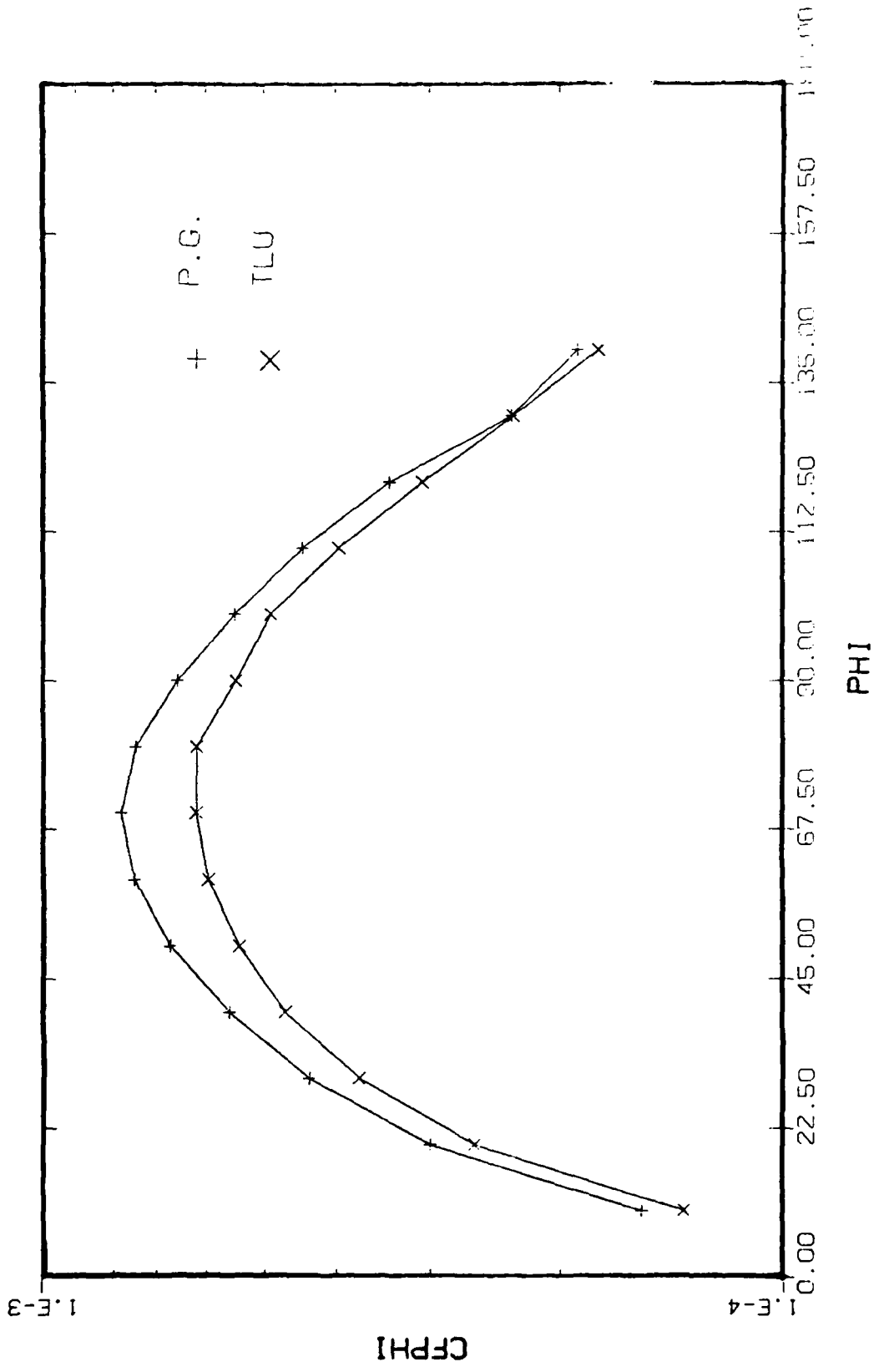


Figure 18. Transverse Variation of $C_{f\phi}$ at $S/R = 20$
 (Case C, $\alpha = 10$ deg, Alt = 80,000 ft, $T_w = \text{Adiabatic}$)

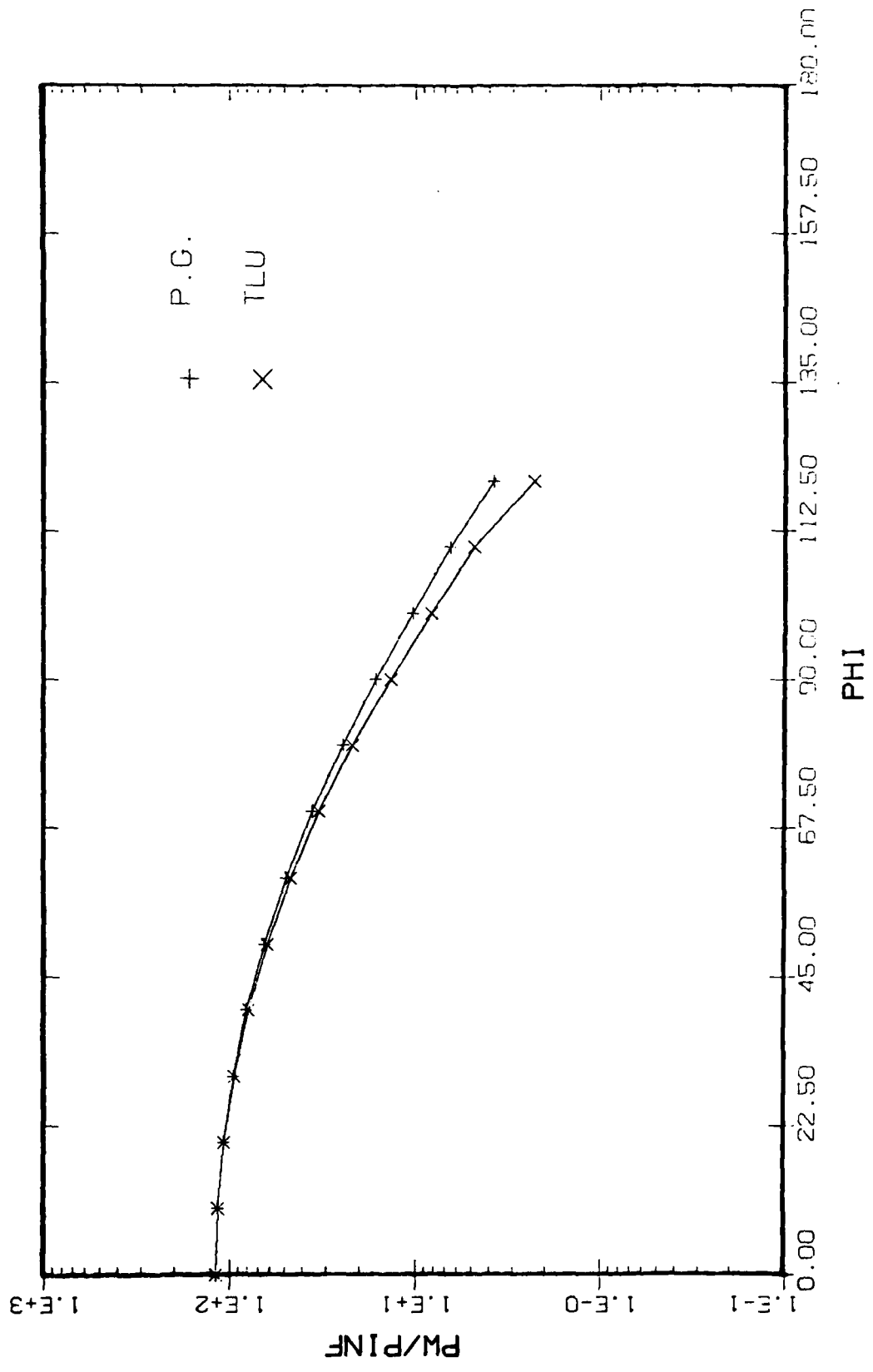


Figure 19. Transverse Variation of Wall Pressure at S/R = 20
 (Case D, $\alpha = 20$ deg, Alt = 80,000 ft, $T_w = 540R$)

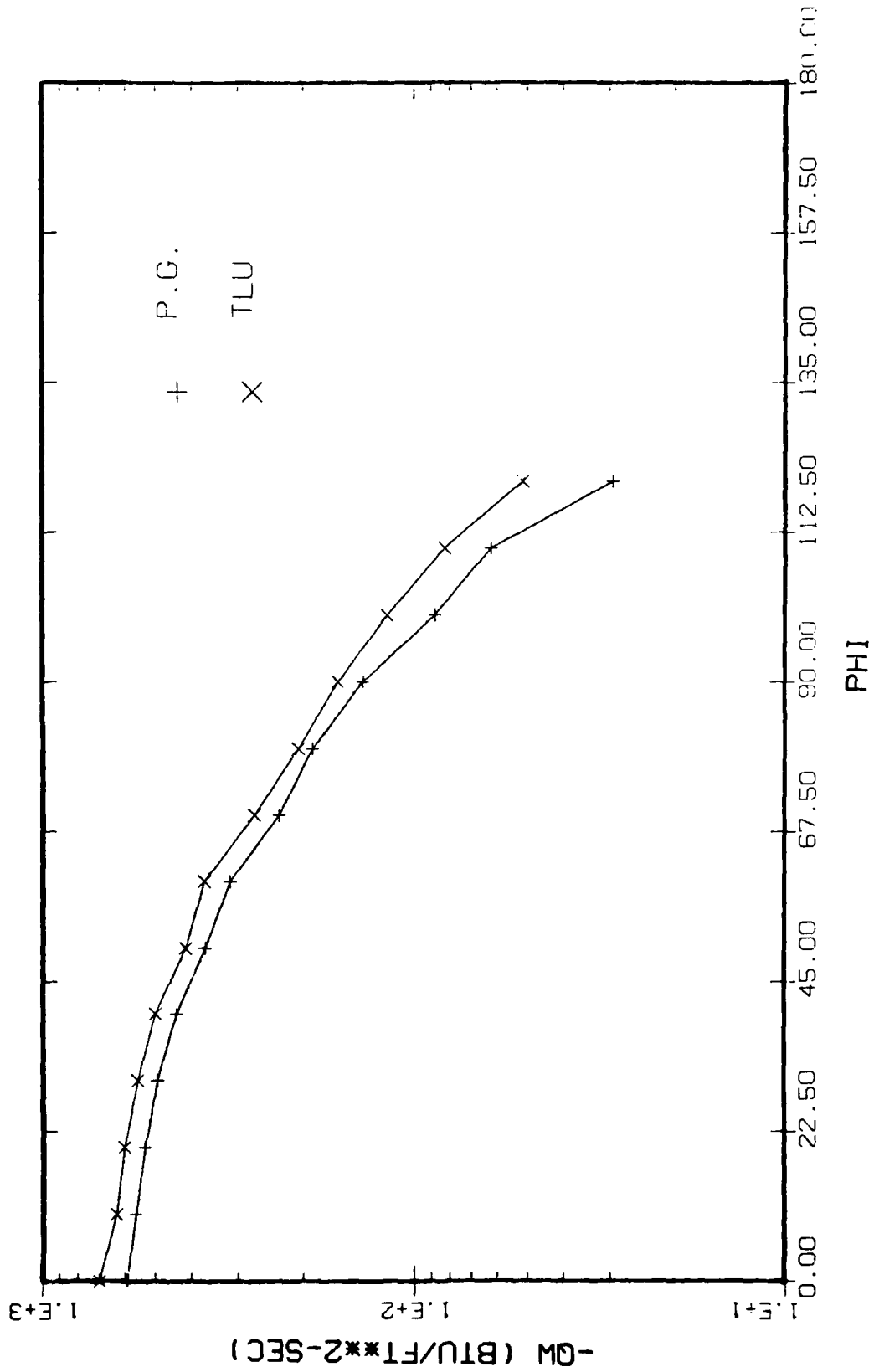


Figure 20. Transverse Variation of Wall Heat-Transfer Rate at S/R = 20
 (Case D, $\alpha = 20$ deg, Alt = 80,000 ft, $T_w = 540R$)

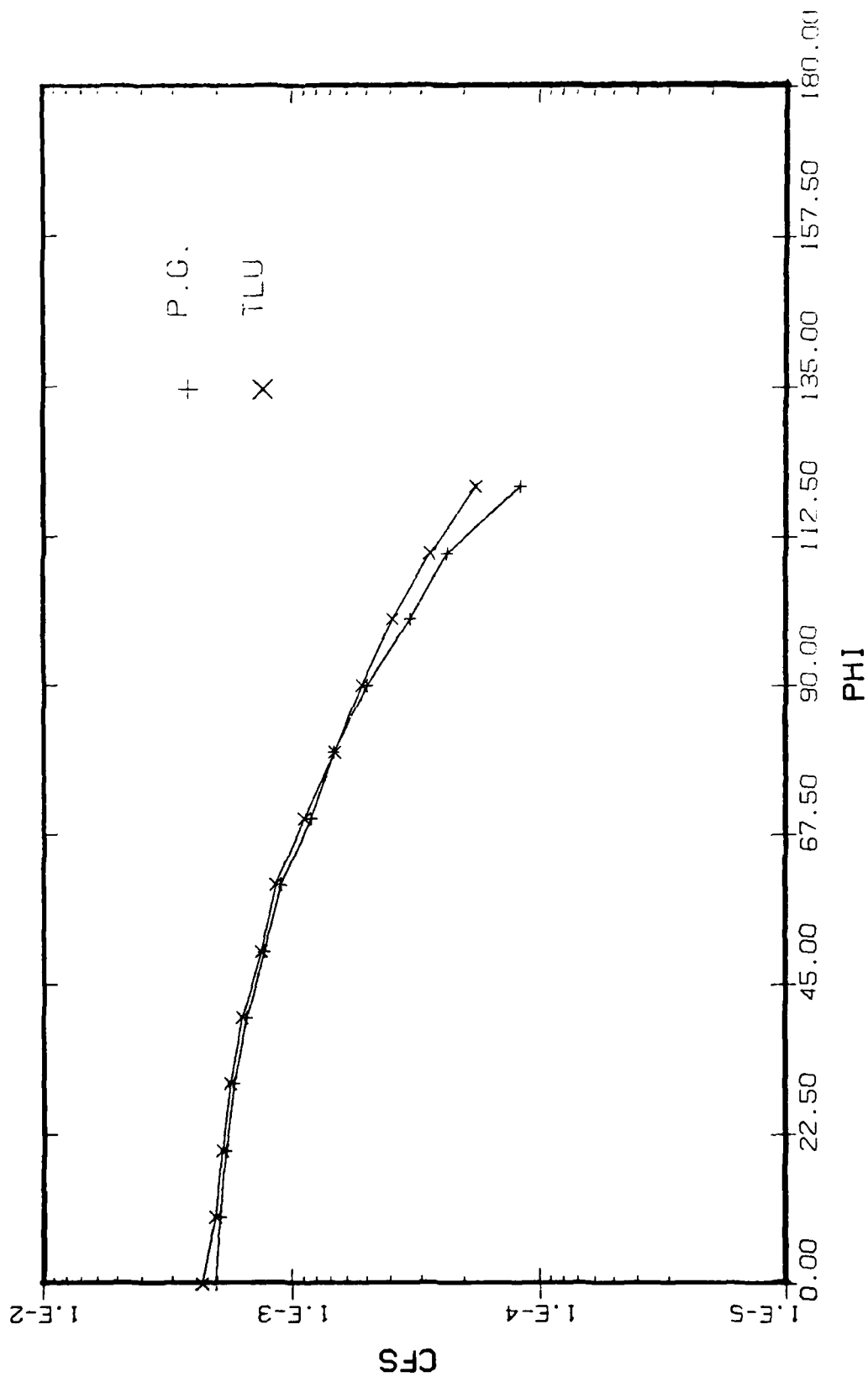


Figure 21. Transverse Variation of C_{fs} at $S/R = 20$
 (Case D, $\alpha = 20$ deg, Alt = 80,000 ft, $T_w = 540R$)

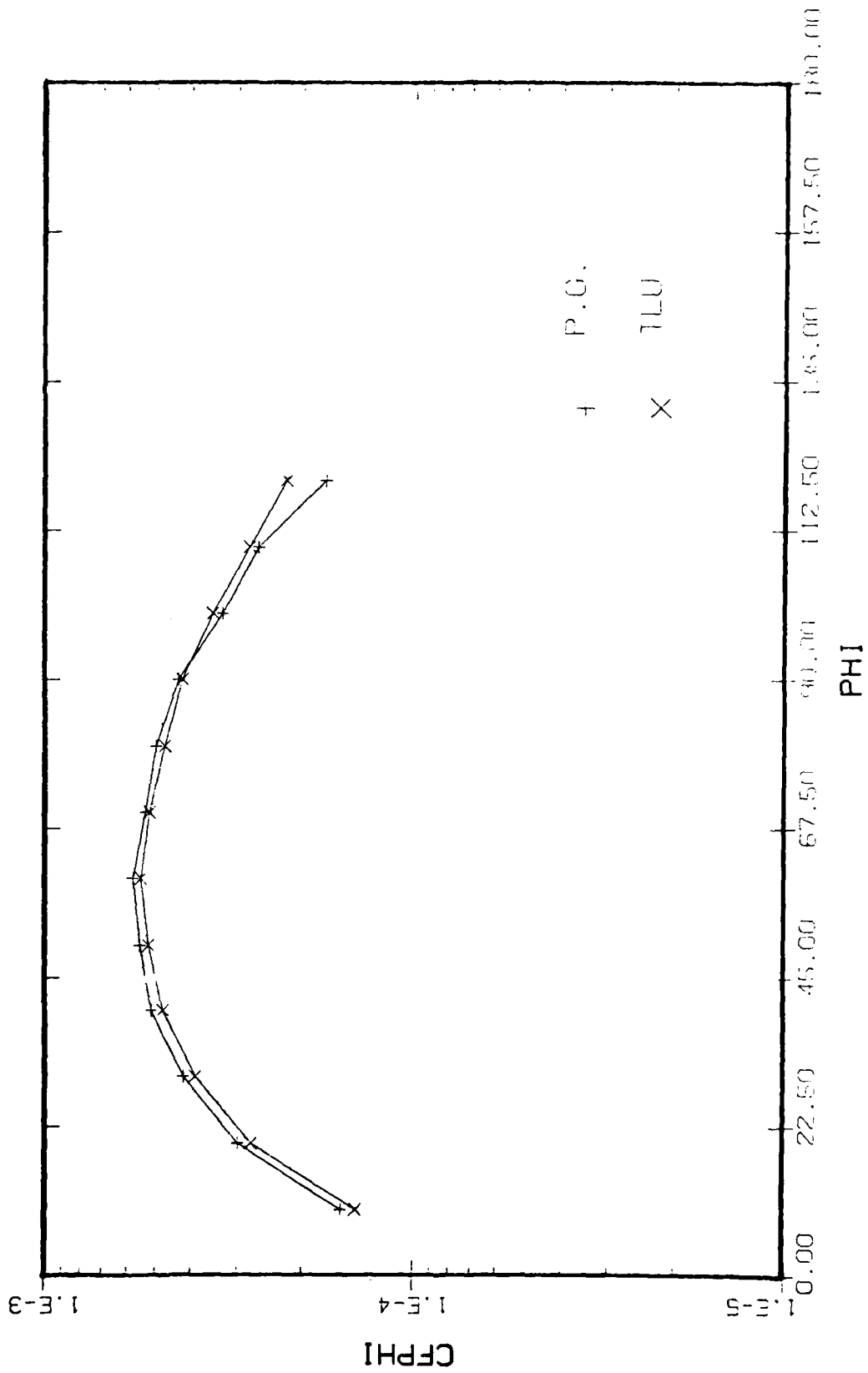


Figure 22. Transverse Variation of $C_{f_{\phi}}$ at $S/R = 20$
 (Case D, $\alpha = 20$ deg, $\Delta t = 80,000$ ft, $T_w = 540R$)